9 Optical Properties

The interaction of semiconductors with light is of decisive importance for photonic and optoelectronic devices as well as for the characterization of semiconductor properties.

9.1 Spectral Regions and Overview

When light hits a semiconductor first reflection, transmission and absorption are considered, as for any dielectric material. The response of the semiconductor largely depends on the photon energy (or wavelength) of the light. In Table 9.1 an overview of the electromagnetic spectrum in the optical range is shown. The energy and wavelength of a photon are related by[1] $E = h\nu = hc/\lambda$, i.e.

$$E\,[\mathrm{meV}] = \frac{1240}{\lambda\,[\mathrm{nm}]}\,. \tag{9.1}$$

Table 9.1. Spectral ranges with relevance to semiconductor optical properties

Range		wavelengths	energies
deep ultraviolet	DUV	$< 250\,\mathrm{nm}$	$> 5\,\mathrm{eV}$
ultraviolet	UV	250–400 nm	3–5 eV
visible	VIS	400–800 nm	1.6–3 eV
near infrared	NIR	800 nm–2 µm	0.6–1.6 eV
mid-infrared	MIR	2–20 µm	60 meV–0.6 eV
far infrared	FIR	20–80 µm	1.6–60 meV
THz region	THz	$> 80\,\mu\mathrm{m}$	$< 1.6\,\mathrm{meV}$

[1] The exact numerical value in (9.1) is 1239.84.

M. Grundmann, *The Physics of Semiconductors*, 2nd ed., Graduate Texts in Physics, DOI 10.1007/978-3-642-13884-3_9,

9.2 Reflection and Diffraction

From Maxwell's equations and the boundary conditions at a planar interface between two media with different index of refraction for the components of the electric and magnetic fields the laws for reflection and diffraction are derived. We denote the index of refraction as n and also n_r in the following. The interface between two media with refractive indices n_1 and n_2 is depicted in Fig. 9.1. In the following we assume first that no absorption occurs.

Snellius' law for the angle of diffraction is

$$n_1 \sin\phi = n_2 \sin\psi \; . \tag{9.2}$$

When the wave enters the denser medium, it is diffracted towards the normal. If the wave propagates into the less-dense medium (reversely to the situation shown in Fig. 9.1), a diffracted wave occurs only up to a critical angle of incidence

$$\sin\phi_\mathrm{TR} = \frac{n_2}{n_1} \; . \tag{9.3}$$

For larger angles of incidence, total internal reflection occurs and the wave remains in the denser medium. Thus, the angle in (9.3) is called the critical angle for total reflection. For GaAs and air the critical angle is rather small, $\phi_\mathrm{TR} = 17.4°$.

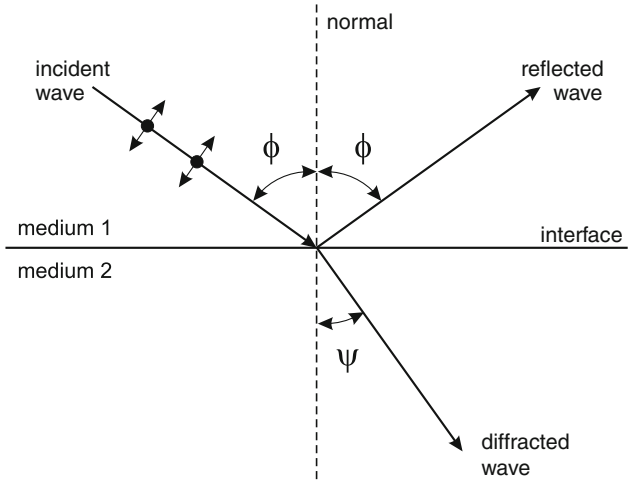

Fig. 9.1. Reflection and diffraction of an electromagnetic wave at the transition between medium '1' and '2', $n_2 > n_1$. The polarization plane is defined by the surface normal and the k-vector of the light (plane of incidence). The parallel ('p') polarized wave (TM-wave, electric field vector oscillates in the plane) is shown as '↔'; perpendicular ('s') polarization (TE-wave, electric field vector is perpendicular to plane) is depicted as '·'

The reflectance depends on the polarization (Fresnel formulas). The index 'p' ('s') denotes parallel polarized/TM (perpendicular polarized/TE) waves.

$$R_{\mathrm{p}} = \left(\frac{\tan(\phi - \psi)}{\tan(\phi + \psi)}\right)^2 \tag{9.4}$$

$$R_{\mathrm{s}} = \left(\frac{\sin(\phi - \psi)}{\sin(\phi + \psi)}\right)^2 . \tag{9.5}$$

The situation for GaAs and air is shown for both polarization directions and unpolarized radiation in Fig. 9.2 for a wave going into and out of the GaAs.

When the reflected and the diffracted wave are perpendicular to each other, the reflectance of the p-polarized wave is zero. This angle is the Brewster angle ϕ_{B},

$$\tan \phi_{\mathrm{B}} = \frac{n_2}{n_1} . \tag{9.6}$$

If a wave has vertical incidence from vacuum on a medium with index of refraction n_{r}, the reflectance is given (both polarizations are degenerate) as

$$R = \left(\frac{n_{\mathrm{r}} - 1}{n_{\mathrm{r}} + 1}\right)^2 . \tag{9.7}$$

For GaAs, the reflectance for vertical incidence is 29.2%.

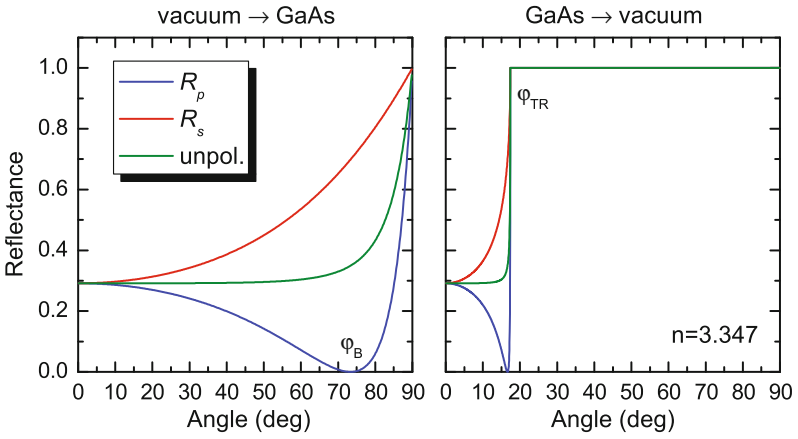

Fig. 9.2. Reflectance of the GaAs/vacuum interface (close to the band gap, $n_{\mathrm{r}} = 3.347$) for radiation from vacuum/air (*left panel*) and from the GaAs (*right panel*), respectively, as a function of incidence angle and polarization

9.3 Absorption

In the absorption process, energy is transferred from the electromagnetic field to the semiconductor. In the case of a linear absorption process, when the probability of light absorption is proportional to the incoming intensity, the decrease of intensity in the absorbing medium is exponential (Lambert–Beer's law [564, 565]),[2]

$$I(x) = I(0)\, \exp -\alpha x \; . \tag{9.8}$$

The quantity α is the *absorption coefficient*, its reverse the absorption depth. The spectral dependence $\alpha(E)$, the absorption spectrum, contains the information of the possible absorption processes, their energy, momentum and angular momentum selection rules, and their strength (oscillator strength).

In Fig. 9.3 a schematic absorption spectrum of a semiconductor is depicted. The transition of electrons from the valence to the conduction band is at the band gap energy. The band gaps of Si, Ge, GaAs, InP, InAs, InSb are in the IR, those of AlAs, GaP, AlP, InN in the VIS, those of GaN and ZnO in the UV, MgO and AlN are in the deep UV. The Coulomb correlation of electrons and holes leads to the formation of excitons that leads to absorption below the band gap. The typical exciton binding energy is in the range of 1–100 meV (see Fig. 9.16). Optical transitions from valence-band electrons into donors and from electrons on acceptors into the conduction band lead to band–impurity absorption. In the region from 10–100 meV the interaction with lattice vibrations (phonons) leads to absorption if the phonons are infrared active. Further in the FIR are transitions from impurities to the closest

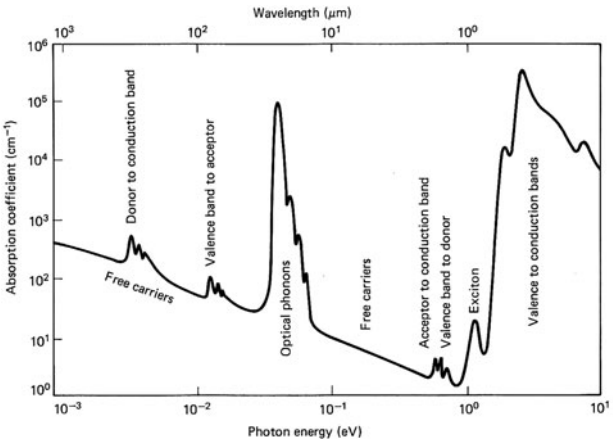

Fig. 9.3. Schematic absorption spectrum of a typical semiconductor. From [566]

[2] In [565], the absorption coefficient μ was defined via $I(d)/I(0) = \mu^d$, i.e. $\mu = \exp -\alpha$.

band edge (donor to conduction and acceptor to valence band). A continuous background is due to free-carrier absorption.

If absorption is considered, the reflectance (9.7) needs to be modified. Using the complex index of refraction $n^* = n_\mathrm{r} + \mathrm{i}\kappa$, it is given as

$$R = \left|\frac{n^* - 1}{n^* + 1}\right|^2 = \frac{(n_\mathrm{r} - 1)^2 + \kappa^2}{(n_\mathrm{r} + 1)^2 + \kappa^2} \; . \tag{9.9}$$

The absorption constant κ is related to the absorption coefficient of the plane wave (damping of $\mathbf{E}^2$) by

$$\alpha = 2\frac{\omega}{c}\kappa = \frac{4\pi}{\lambda}\,\kappa = 2\,k\,\kappa \; . \tag{9.10}$$

Here, k and λ denote the respective values in vacuum.

9.4 Electron–Photon Interaction

The absorption process is quantum mechanically described by the coupling of electrons and photons. The process is described with time-dependent perturbation theory. If $\mathbf{H}_\mathrm{em}$ is the perturbation operator (electromagnetic field), the transition probability per time w_fi for electrons from (unperturbed) state 'i' (initial) to state 'f' (final) is given (with certain approximations) by Fermi's golden rule

$$w_\mathrm{fi}(\hbar\omega) = \frac{2\pi}{\hbar}\,|H'_\mathrm{fi}|^2\,\delta(E_\mathrm{f} - E_\mathrm{i} - \hbar\omega) \; , \tag{9.11}$$

where $\hbar\omega$ is the photon energy, E_i (E_f) is the energy of the initial (final) state. H'_fi is the matrix element

$$H'_\mathrm{fi} = \langle \Psi_\mathrm{f}\,|\mathbf{H}'|\,\Psi_\mathrm{i}\rangle \; , \tag{9.12}$$

where Ψ_i (Ψ_f) are the wavefunctions of the unperturbed initial (final) state.

$\mathbf{A}$ is the vector potential for the electromagnetic field, i.e. $\mathbf{E} = -\dot{\mathbf{A}}$, $\mu\mathbf{H} = \nabla \times \mathbf{A}$, $\nabla \cdot \mathbf{A} = 0$ (Coulomb gauge). The Hamiltonian of an electron in the electromagnetic field is

$$\mathbf{H} = \frac{1}{2m}\,(\hbar\mathbf{k} - q\mathbf{A})^2 \; . \tag{9.13}$$

When terms in $\mathbf{A}^2$ are neglected (i.e. two-photon processes), the perturbation Hamiltonian is thus

$$\mathbf{H}_\mathrm{em} = -\frac{q}{m}\mathbf{A}\mathbf{p} = \frac{\mathrm{i}q\hbar}{m}\mathbf{A}\cdot\nabla \approx q\,\mathbf{r}\cdot\mathbf{E} \; . \tag{9.14}$$

The latter approximation is valid for small wavevectors of the electromagnetic wave and is termed the *electric dipole approximation*.

In order to calculate the dielectric function of the semiconductor from its band structure we assume that $\mathbf{A}$ is weak and we can apply (9.11). The transition probability R for the photon absorption rate at photon energy $\hbar\omega$ is then given by[3]

$$R(\hbar\omega) = \frac{2\pi}{\hbar} \int_{\mathbf{k}_c} \int_{\mathbf{k}_v} |\langle c|\mathbf{H}_{em}|v\rangle|^2 \, \delta\left(E_c(\mathbf{k}_c) - E_v(\mathbf{k}_v) - \hbar\omega\right) \mathrm{d}^3\mathbf{k}_c \, \mathrm{d}^3\mathbf{k}_v \,, \tag{9.15}$$

with the Bloch functions $|c\rangle$ and $|v\rangle$ of the conduction and valence band, respectively, as given in (6.39b).

The vector potential is written as $\mathbf{A} = A\hat{\mathbf{e}}$ with a unit vector $\hat{\mathbf{e}}$ parallel to $\mathbf{A}$. The amplitude is connected to the electric-field amplitude $\mathcal{E}$ via

$$A = -\frac{\mathcal{E}}{2\omega} \left[\exp\left(\mathrm{i}(\mathbf{qr} - \omega t)\right) + \exp\left(-\mathrm{i}(\mathbf{qr} - \omega t)\right)\right] \,. \tag{9.16}$$

In the electric-dipole approximation the momentum conservation $\mathbf{q}+\mathbf{k}_v = \mathbf{k}_c$, $\mathbf{q}$ being the momentum of the light wave is approximated by $\mathbf{k}_v = \mathbf{k}_c$. The matrix element is then given by

$$|\langle c|\mathbf{H}_{em}|v\rangle|^2 = \frac{e^2\,|A|^2}{m^2} \, |\langle c|\hat{\mathbf{e}} \cdot \mathbf{p}|v\rangle|^2 \,, \tag{9.17}$$

with

$$\langle c\,|\hat{\mathbf{e}} \cdot \mathbf{p}|v\rangle|^2 = \frac{1}{3}\,|\mathbf{p}_{cv}|^2 = M_b^2 \,, \tag{9.18}$$

and the momentum matrix element $\mathbf{p}_{cv}$ given in (6.38). A $\mathbf{k}$-independent matrix element $|\mathbf{p}_{cv}|^2$ is often used as an approximation. In Fig. 9.4 the matrix elements for valence to conduction band transitions in GaN are shown as a function of $\mathbf{k}$.

In terms of the electric-field amplitude $\mathcal{E}(\omega)$ the transition probability is

$$R(\hbar\omega) = \frac{2\pi}{\hbar} \left(\frac{e}{m\omega}\right)^2 \left|\frac{\mathcal{E}(\omega)}{2}\right|^2 |\mathbf{p}_{cv}|^2 \int_{\mathbf{k}} \delta\left(E_c(\mathbf{k}) - E_v(\mathbf{k}) - \hbar\omega\right) \mathrm{d}^3\mathbf{k} \,. \tag{9.19}$$

If the integration over $\mathbf{k}$ is restricted to those values allowed in unit volume, the power that is lost from the field in unit volume is given by $R\hbar\omega$. The dielectric function $\epsilon = \epsilon_r + \mathrm{i}\epsilon_i$ is given by

$$\epsilon_i = \frac{1}{4\pi\epsilon_0} \left(\frac{2\pi e}{m\omega}\right)^2 |\mathbf{p}_{cv}|^2 \int_{\mathbf{k}} \delta\left(E_c(\mathbf{k}) - E_v(\mathbf{k}) - \hbar\omega\right) \mathrm{d}^3\mathbf{k} \tag{9.20a}$$

$$\epsilon_r = 1 + \int_{\mathbf{k}} \frac{e^2}{\epsilon_0 m \omega_{cv}^2} \, \frac{2|\mathbf{p}_{cv}|^2}{m\hbar\omega_{cv}} \, \frac{1}{1 - \omega^2/\omega_{cv}^2} \, \mathrm{d}^3\mathbf{k} \,, \tag{9.20b}$$

[3] Here we assume that the valence-band states are filled and the conduction-band states are empty. If the conduction-band states are filled and the valence-band states are empty, the rate is that of stimulated emission.

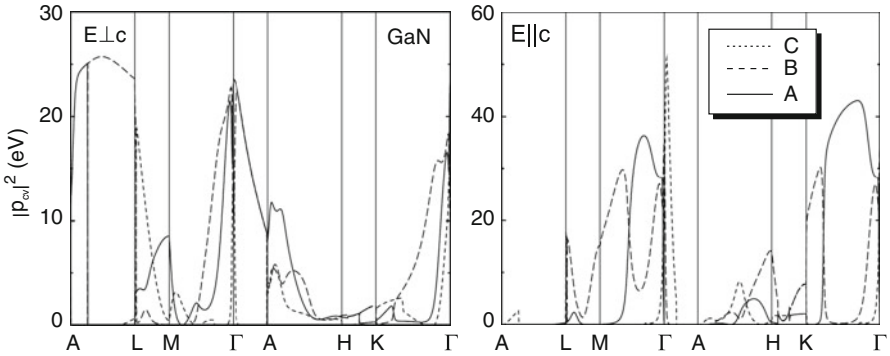

Fig. 9.4. Theoretical momentum matrix elements $|p_{\rm cv}|^2$ along high-symmetry directions in the Brillouin zone (see Fig. 3.32d) for transitions between valence and conduction bands in GaN and light polarized perpendicular (*left panel*) and parallel (*right panel*) to the c-axis. The transitions are A: Γ_9(A)→ Γ_{7c}, B: Γ_7(B)→ Γ_{7c}, C: Γ_7(C)→ Γ_{7c} (see Fig. 6.33). Adapted from [567]

with $\hbar\omega_{\rm cv} = E_{\rm c}(\mathbf{k}) - E_{\rm v}(\mathbf{k})$. The second equation has been obtained via the Kramers–Kronig relations[4] (see Appendix C).

Comparison with (D.7) yields that the oscillator strength of the band–band absorption is given by

$$f = \frac{e^2}{\epsilon_0 m\omega_{\rm cv}^2}\,\frac{2|\mathbf{p}_{\rm cv}|^2}{m\hbar\omega_{\rm cv}}\,, \tag{9.21}$$

with

$$N_{\rm cv} = \frac{2|\mathbf{p}_{\rm cv}|^2}{m\hbar\omega_{\rm cv}} \tag{9.22}$$

being the classical 'number' of oscillators with the frequency $\omega_{\rm cv}$.

9.5 Band–Band Transitions

9.5.1 Joint Density of States

The strength of an allowed optical transitions between valence and conduction bands is proportional to the joint density of states (JDOS) $D_{\rm j}(E_{\rm cv})$ (cf. (6.66), (6.67) and (9.20a))

$$D_{\rm j}(E_{\rm cv}) = 2\int_{S(\tilde{E})} \frac{{\rm d}^2 S}{(2\pi/L)^3}\,\frac{1}{|\nabla_{\mathbf{k}} E_{\rm cv}|}\,, \tag{9.23}$$

[4]The real and imaginary parts of the dielectric function are generally related to each other via the Kramers–Kronig relations.

where E_{cv} is an abbreviation for $E_c(\mathbf{k}) - E_v(\mathbf{k})$ and d^2S is a surface element of the constant energy surface with $\tilde{E} = E_{cv}$. The spin is assumed to generate doubly degenerate bands and accounts for the pre-factor 2. Singularities of the JDOS (*van-Hove singularities* or *critical points*) appear where $\nabla_{\mathbf{k}} E_{cv}$ vanishes. This occurs when the gradient for both bands is zero or when both bands are parallel. The latter generates particularly large JDOS because the condition is valid at many points in $\mathbf{k}$-space.

Generally, the (three-dimensional) energy dispersion $E(\mathbf{k})$ around a three-dimensional critical point (here developed at $\mathbf{k} = 0$) can be written as

$$E(\mathbf{k}) = E(0) + \frac{\hbar^2 k_x^2}{2m_x} + \frac{\hbar^2 k_y^2}{2m_y} + \frac{\hbar^2 k_z^2}{2m_z} \,. \tag{9.24}$$

The singularities are classified as M_0, M_1, M_2 and M_3 with the index being the number of masses m_i in (9.24) that are negative. M_0 (M_3) describes a minimum (maximum) of the band separation. M_1 and M_2 are saddle points. For a two-dimensional $\mathbf{k}$-space there exist M_0, M_1 and M_2 points (minimum, saddle point and maximum, respectively). For a one-dimensional $\mathbf{k}$-space there exist M_0 and M_1 points (minimum and maximum, respectively). The functional dependence of the JDOS at the critical points is summarized in Table 9.2. The resulting shape of the dielectric function is visualized in Fig. 9.5.

9.5.2 Direct Transitions

Transitions between states at the band edges at the Γ point are possible (Fig. 9.6). The $\mathbf{k}$ conservation requires (almost) vertical transitions in the $E(\mathbf{k})$ diagram because the length of the light $\mathbf{k}$ vector, $k = 2\pi/\lambda$, is much

Table 9.2. Functional dependence of the joint density of states for critical points in 3, 2 and 1 dimensions. E_0 denotes the energy (band separation) at the critical point, C stands for a constant value. The type of critical point is given (min.: minimum, saddle: saddle point, max.: maximum)

Dim.	label	type	D_j for $E < E_0$	D_j for $E > E_0$
3D	M_0	min.	0	$\sqrt{E - E_0}$
	M_1	saddle	$C - \sqrt{E_0 - E}$	C
	M_2	saddle	C	$C - \sqrt{E - E_0}$
	M_3	max.	$\sqrt{E_0 - E}$	0
2D	M_0	min.	0	C
	M_1	saddle	$-\ln(E_0 - E)$	$-\ln(E - E_0)$
	M_2	max.	C	0
1D	M_0	min.	0	$\sqrt{E - E_0}$
	M_1	max.	$\sqrt{E_0 - E}$	0

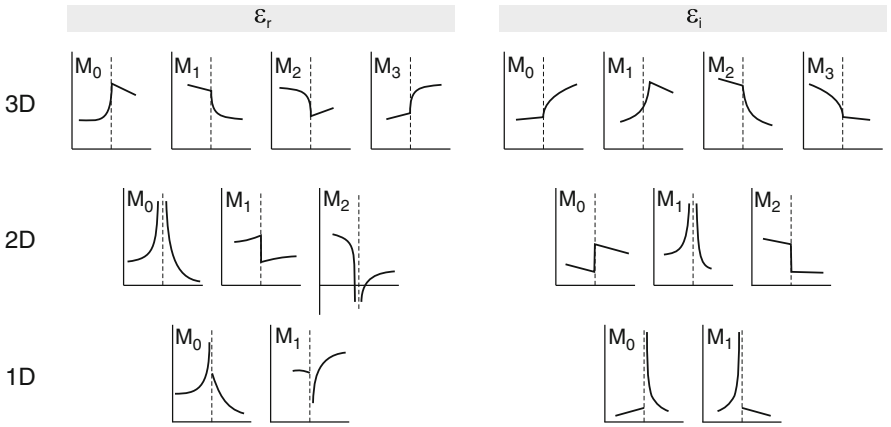

Fig. 9.5. Shape of the real (*left panel*) and imaginary (*right panel*) parts of the dielectric function in the vicinity of critical points in 3, 2 and 1 dimensions (for labels see Table 9.2). The *dashed line* in each graph indicates the energy position of the critical point E_0. Adapted from [568]

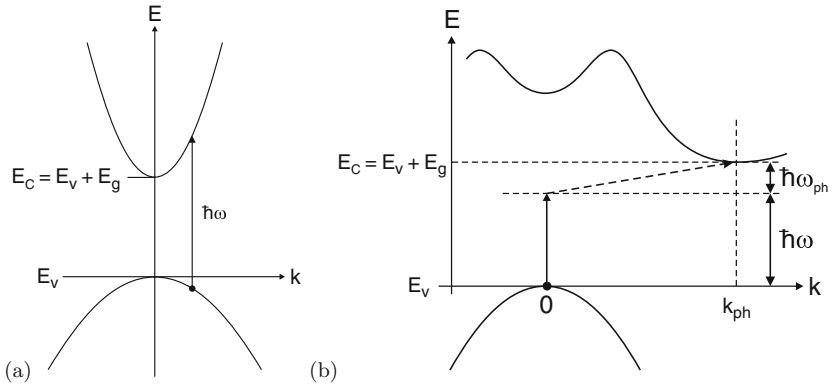

Fig. 9.6. (**a**) Direct optical transition and (**b**) indirect optical transitions between valence and conduction bands. The photon energy is $\hbar\omega$. The indirect transition involves a phonon with energy $\hbar\omega_{\mathrm{ph}}$ (here: phonon absorption) and wavevector k_{ph}

smaller than the size of the Brillouin zone $|k| \leq \pi/a_0$. The ratio of the lengths of the **k** vectors is $\sim 2a_0/\lambda$ and typically about 10^{-3} for NIR wavelengths.

For parabolic bands, i.e. bands described with an energy-independent effective mass, the absorption coefficient is (M_0 critical point)

$$\alpha \propto \sqrt{E - E_{\mathrm{g}}}\,. \tag{9.25}$$

The absorption spectrum of GaAs is shown in Fig. 9.7a for photon energies close to the band gap. The rapid increase, typical for direct semiconductors,

is obvious. At low temperatures, however, the absorption lineshape close to the band gap is dominated by an excitonic feature, discussed in Sect. 9.5.7.

Due to the increasing density of states, the absorption increases with the photon energy (Fig. 9.7c). At 1.85 eV there is a step in the absorption spectrum of GaAs due to the beginning of the contribution of transitions between the s-o hole band and the conduction band (see $E_0 + \Delta_0$ transition in Fig. 9.7e). When bands go parallel, i.e. with the same separation, in the $E(\mathbf{k})$ diagram, the absorption processes contribute at the same transition energy. In this way higher peaks in the absorption spectrum due to the E_1 or E_0' transitions originate as indicated in the band structure in Fig. 9.7e.

The selection rules for transitions from valence to conduction band must take into account the angular momentum and spin states of the wavefunctions. The optical transitions are circularly polarized as shown in Fig. 9.8. A lifting of the energetic degeneracies of these states occurs, e.g. by magnetic fields or spatial confinement.

9.5.3 Indirect Transitions

In an indirect band structure the missing k difference (across the Brillouin zone) between valence- and conduction-band state needs to be provided by a second particle. A phonon can provide the momentum and additionally contributes a small amount of energy $\hbar\omega_{\mathrm{ph}}$. There are several steps in the absorption spectrum due to various involved phonons (or combinations of them). At low temperature ($T = 1.6$ K, Fig. 9.9) phonons can only be generated and the absorption starts at energies *above* the band gap. At higher temperatures (typically above 40 K [569], Fig. 9.9), acoustical phonons assisting the optical absorption transition can also be absorbed from the crystal; in this case due to energy conservation the absorption starts already at an energy $E_{\mathrm{g}} - \hbar\omega_{\mathrm{ph}}$ *below* the band gap. At even higher temperatures (> 200 K, Fig. 9.9), also optical phonons can be absorbed.

The two-particle process is less probable than the direct absorption that only involves one photon. The perturbation calculation yields an absorption coefficient with a quadratic dependence on energy (9.26) [570]. However, the strength close to the band gap is about 10^{-3} smaller than for the direct transition.

$$\alpha \propto (E - E_{\mathrm{g}} \pm \hbar\omega_{\mathrm{ph}})^2 \,. \tag{9.26}$$

An 11-parameter formula based on terms like (9.26) can describe the room temperature absorption spectrum of silicon in the visible with a precision of a few percent [573].

The absorption spectra close to the absorption edge are shown for GaP (Fig. 9.9) and Si (Fig. 9.10a). According to (9.26), the plot of $\sqrt{\alpha}$ vs. energy (Macfarlane-Roberts plot [574]) yields a straight line beyond the spectral region of phonon effects. The complicated form close to the (indirect) gap energy is due to the contribution of different phonons. The phonon energies

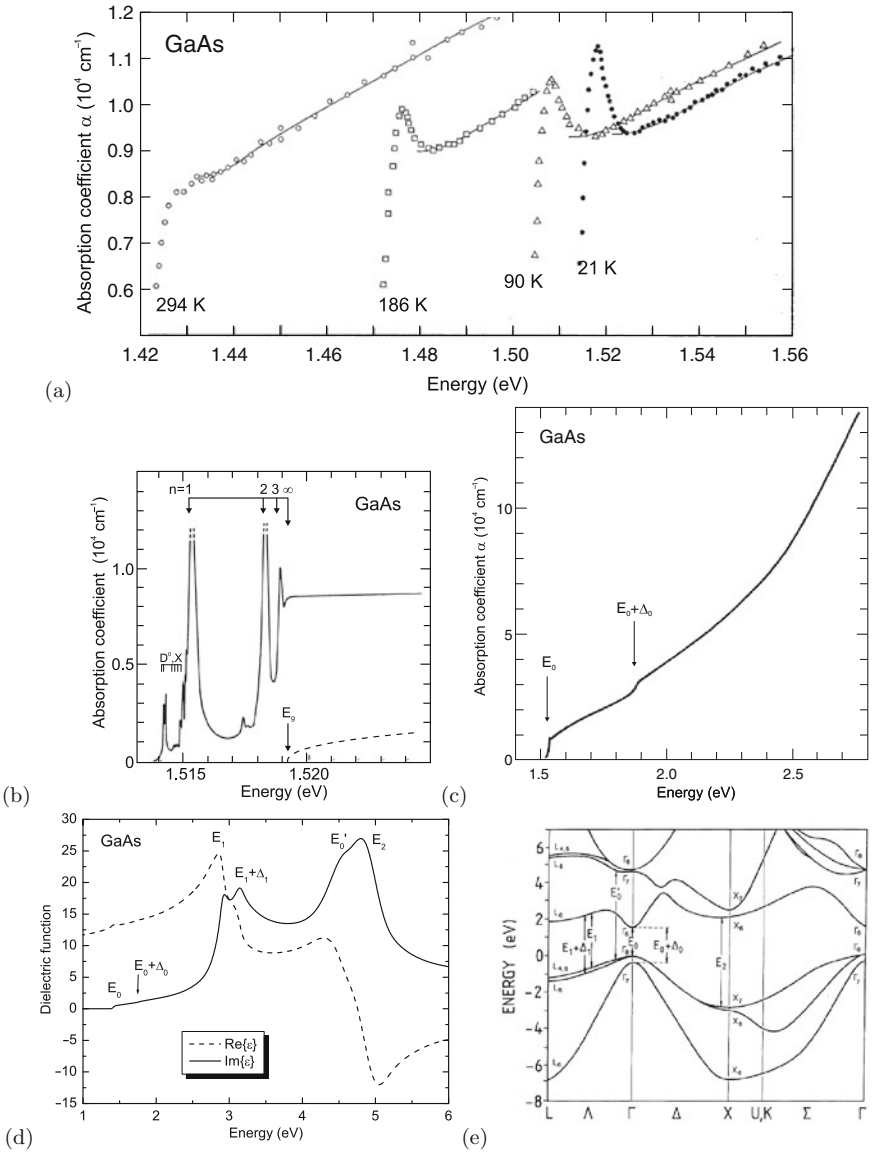

Fig. 9.7. (**a**) Absorption of GaAs close to the band gap at different temperatures. Adapted from [571]. (**b**) High-resolution absorption spectrum of highly pure GaAs at $T = 1.2\,\mathrm{K}$ in the exciton region. *Dashed line* is theory without excitonic correlation. Adapted from [572]. (**c**) Absorption spectrum of GaAs at $T = 21\,\mathrm{K}$ in the vicinity of the band gap. Adapted from [571]. (**d**) Complex dielectric function of GaAs at $T = 300\,\mathrm{K}$, *dashed* (*solid*) *line*: real (imaginary) part of dielectric constant. Peak labels relate to transitions shown in part (**e**). (**e**) Band structure of GaAs with band gap transition (E_0) and higher transitions ($E_0 + \Delta_0$, E_1, $E_1 + \Delta_1$, E_0', and E_2) indicated

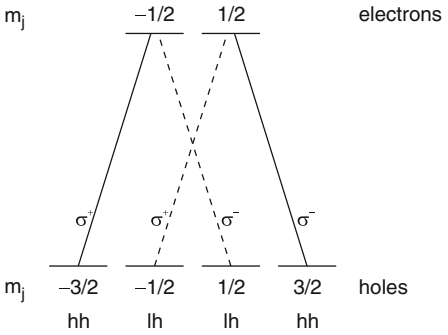

Fig. 9.8. Optical selection rules for band–band transitions in bulk material

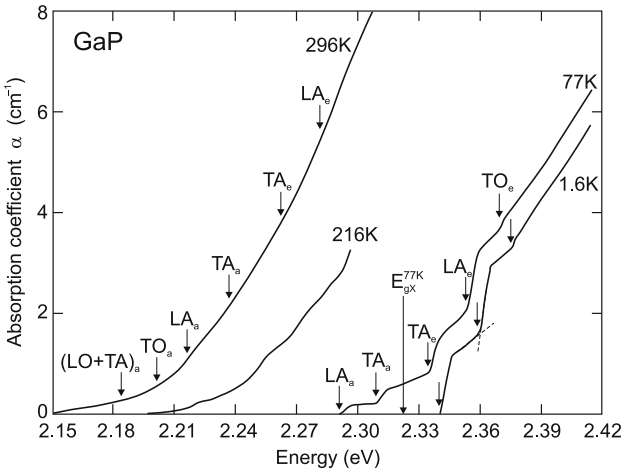

Fig. 9.9. Absorption edge of GaP at various temperatures. The index 'e' ('a') indicates phonon emission (absorption) during the optical absorption process. The theoretical excitonic gap (E_{gX}) at $T = 77\,\mathrm{K}$ is indicated Adapted from [569]

found to contribute to the silicon absorption edge [575] agree with the TA and TO energy at the X minimum [576] (Fig. 9.10b). Also multiple phonons can contribute (Fig. 9.9). The momentum conservation can also be achieved by impurity scattering or electron-electron scattering [577].

We note also that the indirect semiconductors have an optical transition between Γ valence- and conduction-band states. However, this transition is at higher energies than the fundamental band gap, e.g. for Si ($E_{\mathrm{g}} = 1.12\,\mathrm{eV}$) at 3.4 eV (see Fig. 6.5a). In Fig. 9.11, the absorption scheme for indirect and direct absorption processes starting with an electron at the top of the valence band is shown together with an experimental absorption spectrum for Ge with the direct transition ($\Gamma_8 \rightarrow \Gamma_7$) at 0.89 eV, 0.136 eV above the fundamental band gap.

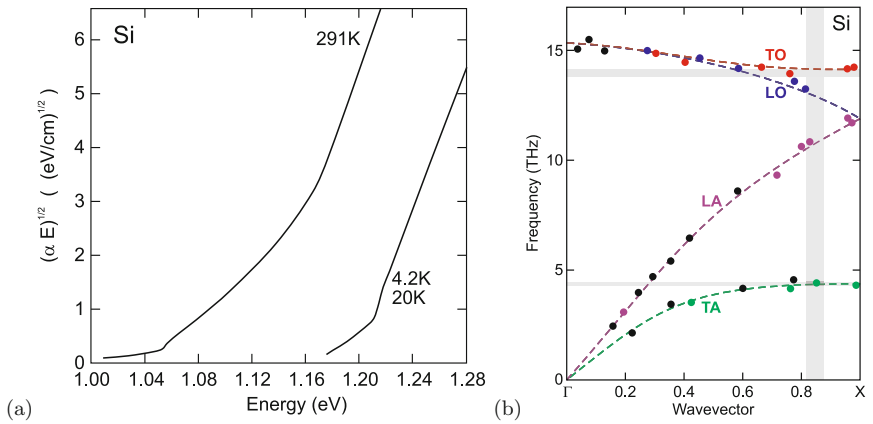

Fig. 9.10. (**a**) Absorption edge of Si at two different temperatures. Adapted from [575]. (**b**) Phonon energies in silicon along [001] obtained from neutron scattering (*black*: unidentified, *green*: TA, *purple*: LA, *blue*: LO, *red*: TO). The *vertical grey bar* indicates the position of the conduction band minimum, the *horizontal grey bars* the energies of the phonons observed at the indirect optical absorption edge. The *dark grey* overlap areas indicate that TO and TA phonons contribute. Adapted from [576]

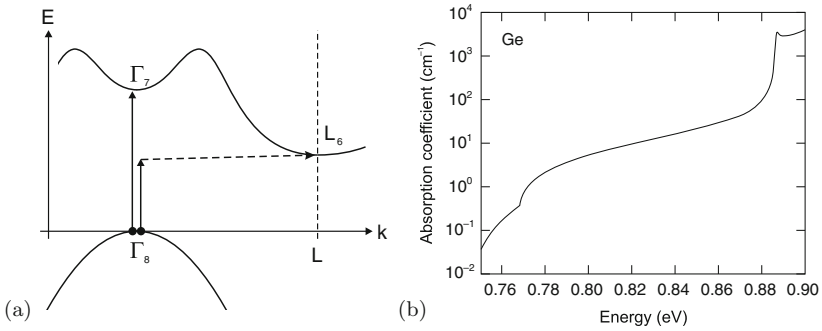

Fig. 9.11. (**a**) Scheme of indirect and direct optical transitions starting at the top of the valence band in Ge. Vertical *solid lines* represent the involved photon, the horizontal *dashed line* the involved phonon. (**b**) Experimental absorption spectrum of Ge ($T = 20\,\mathrm{K}$). Adapted from [575]

In Fig. 9.12, the absorption edge of $BaTiO_3$ is shown. An indirect transition with an increase of (weak) absorption $\propto E^2$ and an indirect gap of $E_\mathrm{i} = 2.66\,\mathrm{eV}$ and a direct transition with an increase of (strong) absorption $\propto E^{1/2}$ and a direct gap of $E_\mathrm{d} = 3.05\,\mathrm{eV}$ are observed. These transitions could be due to holes at the M (indirect gap) and Γ (direct gap) points (cf. Sect. 6.3.9), respectively.

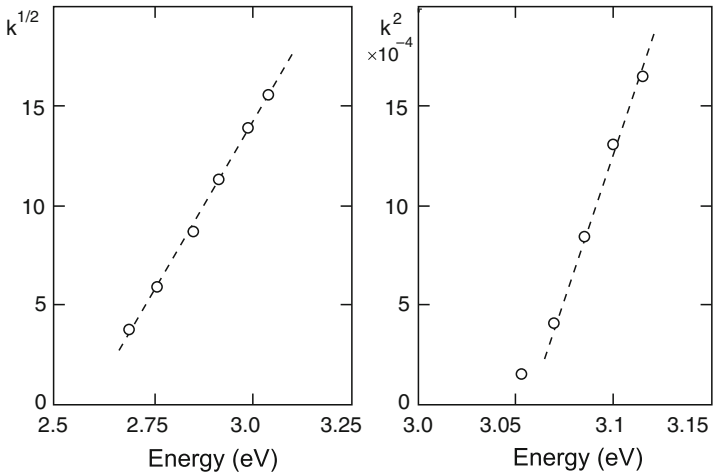

Fig. 9.12. Absorption of $BaTiO_3$ at room temperature. Experimental data (*circles*) from [578] with fits (*dashed lines*) $\propto E^2$ and $\propto E^{1/2}$, respectively

9.5.4 Urbach Tail

Instead of the ideal $(E - E_g)^{1/2}$ dependence of the direct band-edge absorption, often an exponential tail is observed (see Fig. 9.13). This tail is called the Urbach tail [579] and follows the functional dependence

$$\alpha(E) = \alpha_g \exp\left(\frac{E - E_g}{E_0}\right) , \tag{9.27}$$

where E_0 is the characteristic width of the absorption edge, the so-called Urbach parameter.

The Urbach tail is attributed to transitions between band tails below the band edges. Such tails can originate from disorder of the perfect crystal, e.g. from defects or doping, and the fluctuation of electronic energy bands due to lattice vibrations. The temperature dependence of the Urbach parameter E_0 is thus related to that of the band gap as discussed in [581, 582].

9.5.5 Intravalence-Band Absorption

Besides optical interband transitions between the valence and the conduction band there are also optical transitions within the valence band. In p-type material holes from the valence-band edge can undergo absorption and end up in the split-off hole band (Fig. 9.14a). Such intravalence-band absorption occurs at photon energies close to Δ_0 as shown in Fig. 9.14b for p-type GaAs:Zn. Also, hh $\rightarrow$ lh transitions are possible.

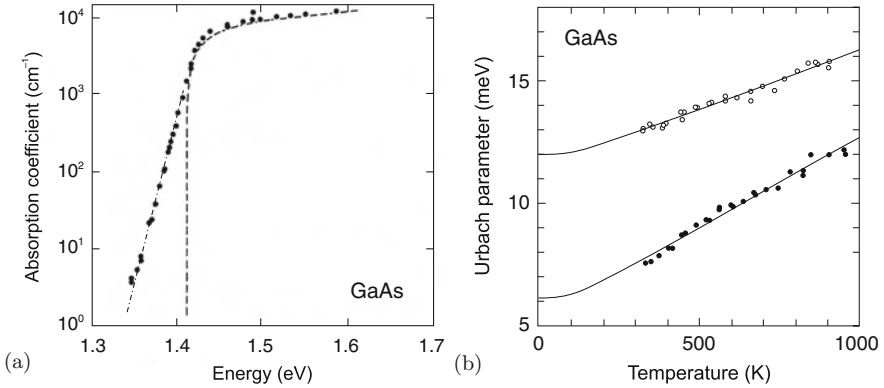

Fig. 9.13. (**a**) Experimental absorption spectrum (*circles*) of GaAs at room temperature on a semilogarithmic plot. The exponential tail below the band gap is called the Urbach tail (the *dash-dotted* line corresponds to $E_0 = 10.3\,\text{meV}$ in (9.27)). The *dashed line* is the theoretical dependence from (9.25). Adapted from [580]. (**b**) Temperature dependence of Urbach parameter E_0 for two GaAs samples. Experimental data for undoped (*solid circles*) and Si-doped ($n = 2 \times 10^{18}\,\text{cm}^{-3}$, *empty circles*) GaAs and theoretical fits (*solid lines*) with one-phonon model. Adapted from [581]

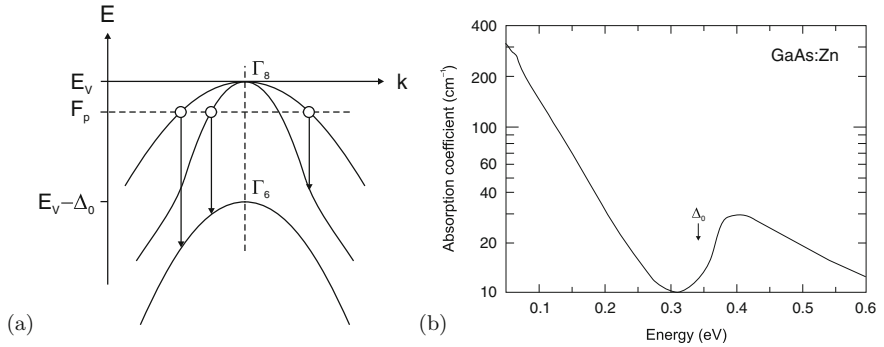

Fig. 9.14. (**a**) Schematic optical transitions within the valence band. Holes (*empty circles*) are shown to start at the hole quasi-Fermi level, transitions are from left to right: 'hh → s-o', 'lh → s-o' and 'hh → lh'. (**b**) Experimental absorption spectrum of GaAs:Zn with $p = 2.7 \times 10^{17}\,\text{cm}^{-3}$ at $T = 84\,\text{K}$. The absorption above the split-off energy Δ_0 is due to the hh/lh → s-o process. Adapted from [583]

9.5.6 Amorphous Semiconductors

The sharp features in the dielectric function due to critical points in the band structure of crystalline semiconductors are washed out in amorphous material. As an example the spectra of the imaginary part of the dielectric function for crystalline (trigonal) and amorphous selenium are shown in Fig. 9.15.

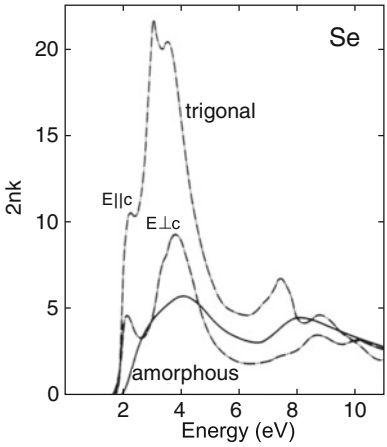

Fig. 9.15. Imaginary part of the dielectric function of amorphous (*solid line*) and crystalline (trigonal) selenium (*dash-dotted lines* for two different polarization directions). From [584]

9.5.7 Excitons

An electron in the conduction band and a hole in the valence band form a hydrogen-like state due to the mutual Coulomb interaction. Such a state is called an exciton. The center-of-mass motion is separated and has a dispersion $E = \frac{\hbar^2}{2M}\mathbf{K}^2$, where $M = m_\mathrm{e} + m_\mathrm{h}$ is the total mass and $\hbar\mathbf{K}$ is the center-of-mass momentum

$$\mathbf{K} = \mathbf{k}_\mathrm{e} + \mathbf{k}_\mathrm{h} \; . \tag{9.28}$$

The relative motion yields hydrogen-like quantized states $E_n \propto n^{-2}$ $(n \geq 1)$:

$$E_\mathrm{X}^n = -\frac{m_\mathrm{r}^*}{m_0}\,\frac{1}{\epsilon_\mathrm{r}^2}\,\frac{m_0 e^4}{2(4\pi\epsilon_0\hbar)^2}\,\frac{1}{n^2} \; , \tag{9.29}$$

where m_r^* denotes the reduced effective mass $m_\mathrm{r}^{*-1} = m_\mathrm{e}^{*-1} + m_\mathrm{h}^{*-1}$. The third factor is the atomic Rydberg energy (13.6 eV). The exciton binding energy $E_X^b = -E_X^1$ is scaled by $\frac{m^*}{m_0}\frac{1}{\epsilon_\mathrm{r}^2} \approx 10^{-3}$. A more detailed theory of excitons beyond the simple hydrogen model presented here, taking into account the valence-band structure, can be found in [585] for direct and [586] for indirect cubic and in [587] for wurtzite semiconductors. The exciton binding energies for various semiconductors are listed in Table 9.3 and shown in Fig. 9.16a vs. the band gap.

The radius of the exciton is

$$r_\mathrm{X}^n = n^2\,\frac{m_0}{m_\mathrm{r}^*}\,\epsilon_\mathrm{r}\,a_\mathrm{B} \; , \tag{9.30}$$

Table 9.3. Exciton (E_X^b) and biexciton (E_{XX}^b, see Sect. 9.5.11) binding energies in various bulk semiconductors. Values for 10 nm GaAs/15 nm $Al_{0.3}Ga_{0.7}As$ quantum well (QW) are taken from [588]

Material	E_X^b (meV)	E_{XX}^b (meV)	E_{XX}^b/E_X^b
GaAs	4.2		
GaAs QW	9.2	2.0	0.22
ZnSe	17	3.5	0.21
GaN	25	5,6	0.22
CdS	27	5.4	0.20
ZnS	37	8.0	0.22
ZnO	59	15	0.25

where $a_B = 0.053\,\text{nm}$ denotes the hydrogen Bohr radius.[5] The Bohr radius of the exciton is $a_X = r_X^1$ (14.6 nm for GaAs, $\sim 2\,\text{nm}$ for ZnO). The exciton moves with the center-of-mass **K**-vector through the crystal. The complete dispersion is (see Fig. 9.16b)

$$E = E_g + E_X^n + \frac{\hbar^2}{2M}\,\mathbf{K}^2\,. \tag{9.31}$$

The oscillator strength of the exciton states decays $\propto n^{-3}$. The absorption due to excitons is visible in Fig. 9.7a for GaAs at low temperatures. If inhomogeneities are present, typically only the $n = 1$ transition is seen. How-

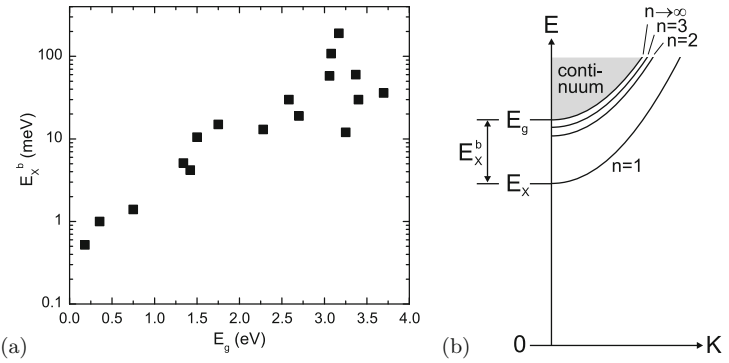

Fig. 9.16. (**a**) Exciton binding energy vs. band gap for various semiconductors. (**b**) Schematic dispersion of excitonic levels. The K-vector refers to the center-of-mass motion

[5] Cf. (7.25); an electron bound to a donor can be considered as an exciton with an infinite hole mass.

ever, under special conditions also higher transitions of the exciton Rydberg series are seen (e.g. $n = 2$ and 3 in Fig. 9.7b).

The exciton concept was introduced first for absorption in Cu_2O [589]. The $J = 1/2$ absorption spectrum ('yellow series') is shown in Fig. 9.17. In this particular material both the valence and conduction bands have s character, thus the 1s transition of the exciton is forbidden and the np transitions are observed in normal (one-photon) absorption. Only with two-photon absorption can the s (and d) transitions also be excited.

The scattering (unbound) states of the exciton [590] for $E > E_g$ contribute to absorption above the band gap. The factor by which the absorption spectrum is changed is called the Sommerfeld factor. For bulk material it is

$$S(\eta) = \eta \frac{\exp(\eta)}{\sinh(\eta)} , \tag{9.32}$$

with $\eta = \pi \left(\frac{E_X^b}{E - E_g} \right)^{1/2}$. The change of the absorption spectrum due to the Coulomb correlation is shown in Fig. 9.18. There is a continuous absorption between the bound and unbound states. At the band gap there is a finite absorption ($S(E \to E_g) \to \infty$). The detail to which exciton peaks can be resolved depends on the spectral broadening.

In Fig. 9.19 the energy separations of the A-, B-, and C-excitons in GaN are shown [365]. Thus, the ordering of the valence bands depends on the strain state of the semiconductor.

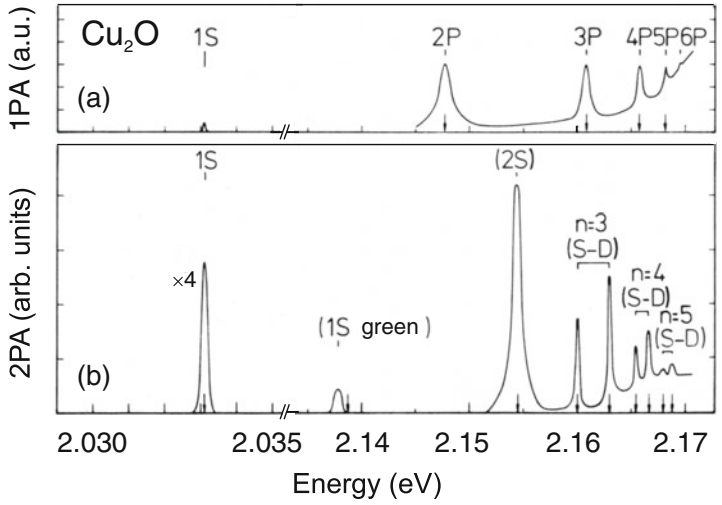

Fig. 9.17. One-photon (*top*) and two-photon (*bottom*) absorption spectra of Cu_2O at $T = 4.2\,K$. *Arrows* denote theoretical peak positions. Adapted from [592]

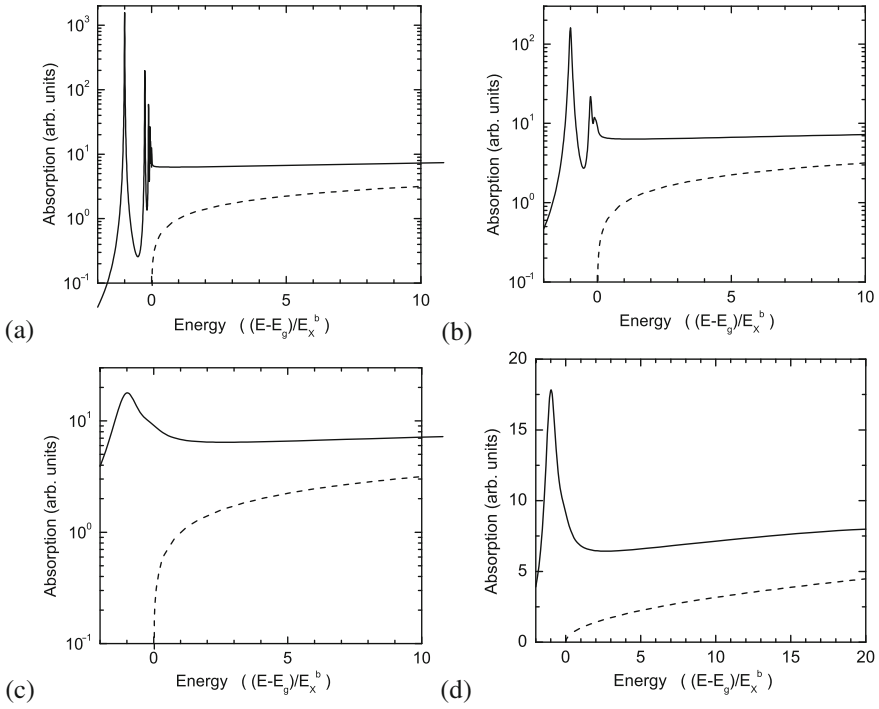

Fig. 9.18. Modification of the absorption edge of a direct transition by excitonic effects for different spectral (Lorentzian) broadening ($\propto (E^2 + \Gamma^2/4)^{-1}$), (**a**) $\Gamma = 0.01 E_{\mathrm{X}}^{\mathrm{b}}$, (**b**) $\Gamma = 0.1 E_{\mathrm{X}}^{\mathrm{b}}$, (**c**) $\Gamma = E_{\mathrm{X}}^{\mathrm{b}}$. (**d**) is (**c**) in linear scale. *Dashed lines* are electron–hole plasma absorption according to (9.25)

9.5.8 Phonon Broadening

The scattering with phonons and the related dephasing leads to homogeneous broadening Γ_{hom} of absorption (and recombination) lines. Acoustic and optical phonons contribute to the broadening according to the dependence [591]

$$\Gamma_{\mathrm{hom}}(T) = \Gamma_0 + \gamma_{\mathrm{AC}}\, T + \gamma_{\mathrm{LO}}\, \frac{1}{\exp(\hbar\omega_{\mathrm{LO}}/kT) - 1}\ , \tag{9.33}$$

where $\hbar\omega_{\mathrm{LO}}$ is the optical phonon energy and the last factor is the Bose function (E.22). Γ_0 is a temperature-independent contribution, $\Gamma_0 = \Gamma(T = 0)$. The increasing broadening with increasing temperature is obvious, e.g., in absorption spectra (Fig. 9.20a). In Fig. 9.20b experimental data for GaAs, ZnSe and GaN are assembled. The data have been fitted with (9.33); the resulting phonon broadening parameters are listed in Table 9.4.[6] The optical

[6] Such parameter can be directly determined from spectroscopic broadening (as in [594]) or a time-resolved measurement of the decay of the coherent polarization

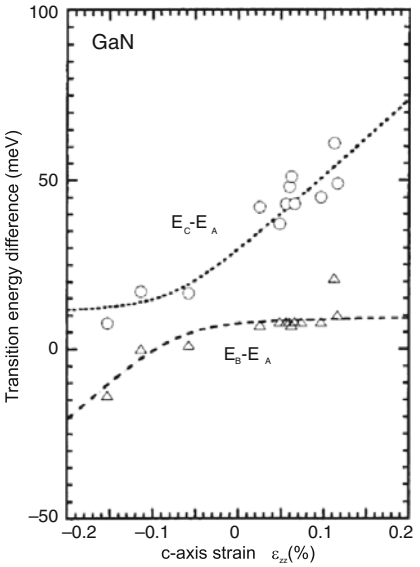

Fig. 9.19. Theoretical dependency (*lines*) for the the differences of the C-line and A-line as well as B-line and A-line exciton transition energies in GaN as a function of the *c*-axis strain. *Symbols* are experimental data from [598]. Adapted from [365]

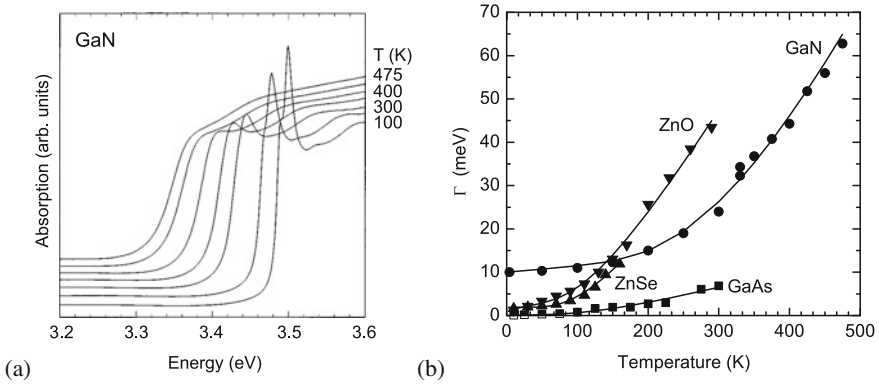

Fig. 9.20. (**a**) Absorption spectra of GaN bulk (0.38 µm thick epilayer on sapphire) for various temperatures $T = 100$, 200, 300, 350, 400, 450, and 475 K. Adapted from [594] (**b**) Homogeneous broadening as a function of temperature, *symbols* are experimental data, *solid lines* are fits, rf. Table 9.4

(four-wave mixing) as in [595]. In the latter, the decay constant of the dephasing T_2 is related to the decay constant τ of the FWM-signal by $T_2 = 2\tau$ for homogeneous broadening. The Fourier transform of $\exp -t/(2\tau)$ is a Lorentzian of the type $\propto ((E - E_0)^2 + \Gamma^2/4)^{-1}$ with $\Gamma = 1/\tau$ being the FWHM.

Table 9.4. Phonon broadening parameters (FWHM) of various bulk semiconductors. Values from fits with (9.33) to experimental data for GaAs [596], ZnSe [595], GaN [594], ZnO [597] (phonon energy fitted) as shown in Fig. 9.21b

Material	$\hbar\omega_{\mathrm{LO}}$ (meV)	Γ_0 (meV)	γ_{AC} (μeV/K)	γ_{LO} (meV)
GaAs	36.8	0	4 ± 2	16.8 ± 2
ZnSe	30.5	1.9	0 ± 7	84 ± 8
GaN	92	10	15 ± 4	408 ± 30
ZnO	33	1.2	32 ± 26	96 ± 24

transitions in polar semiconductors exhibit stronger coupling to optical phonons. The phonon coupling parameters from different measurements on GaN are discussed and compared in [593].

9.5.9 Exciton Polariton

Electrons and holes are particles with spin 1/2. Thus, the exciton can form states with total spin $S = 0$ (para-exciton, singlet) and $S = 1$ (ortho-exciton, triplet). The exchange interaction leads to a splitting of these states, the singlet being the energetically higher. The singlet state splits into the longitudinal and transverse exciton with respect to the orientation of the polarization carried by the Bloch functions and the center-of-mass motion $\mathbf{K}$ of the exciton. Dipole transitions are only possible for singlet excitons (bright excitons). The triplet excitons couple only weakly to the electromagnetic field and are thus also called dark excitons.

The coupling of these states to the electromagnetic field creates new quasiparticles, the exciton polaritons [599, 600]. The dielectric function of the exciton (with background dielectric constant ϵ_{b}) is

$$\epsilon(\omega) = \epsilon_{\mathrm{b}} \left[1 + \frac{\beta}{1 - (\omega^2/\omega_{\mathrm{X}})^2} \right] \cong \epsilon_{\mathrm{b}} \left[1 + \frac{\beta}{1 - (\omega^2/\omega_{\mathrm{T}})^2 + \hbar\, K^2/(M\, \omega_{\mathrm{T}})} \right] , \tag{9.34}$$

where β is the oscillator strength and the energy is $\hbar\omega_{\mathrm{X}} = \hbar\omega_{\mathrm{T}} + \hbar^2\, K^2/2M$. $\hbar\omega_{\mathrm{T}}$ is the energy of the transverse exciton at $K = 0$. With this dispersion the wave dispersion must be fulfilled, i.e.

$$c^2\, k^2 = \omega^2\, \epsilon(\omega) \, , \tag{9.35}$$

where k is the k vector of the light that needs to be $k = K$ due to momentum conservation. The dependence of the dielectric function on k is called *spatial dispersion* [601]. Generally, up to terms in k^2 it is written as

$$\epsilon(\omega) = \epsilon_{\mathrm{b}} \left[1 + \frac{\beta}{1 - (\omega^2/\omega_0)^2 + D\, k^2} \right] \, . \tag{9.36}$$

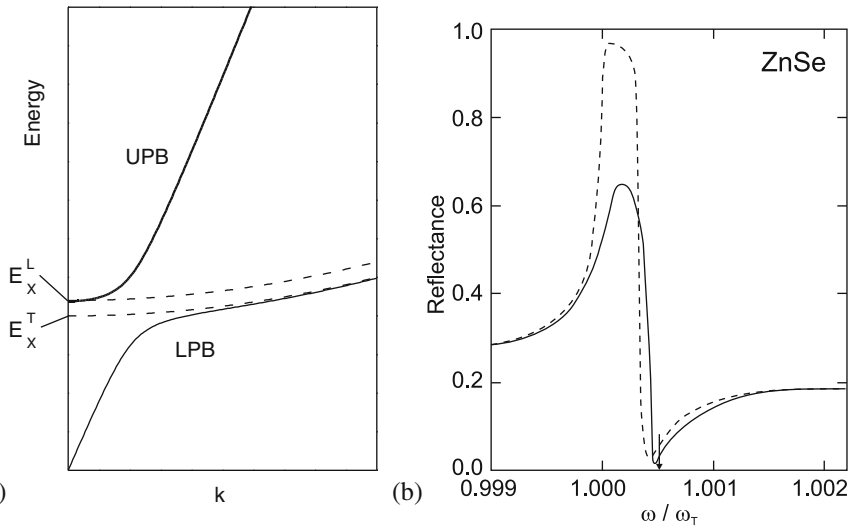

Fig. 9.21. (**a**) Schematic dispersion of exciton polaritons. The lower polariton branch ('LPB') is at small k photon-like, at large k exciton-like. The upper branch ('UPB') is exciton-like at small k and photon-like at larger k. The limit of the UPB for $k \to 0$ is the energy of the longitudinal exciton. The *dashed lines* represent the pure exciton dispersions. (**b**) Theoretical effect of spatial dispersion on the reflectance at the fundamental exciton resonance at normal incidence for ZnSe material parameters ($\hbar\omega_T$ =2.8 eV, $\beta = 1.0 \times 10^{-3}$ and a background dielectric constant of $\epsilon_b = 8.1$, damping was set to $\Gamma = 10^{-5}\omega_T$). The arrow denotes the position of ω_L. The *solid* (*dashed*) *line* is with (without) spatial dispersion for $\hat{D} = 0.6 \times 10^{-5}$ ($\hat{D} = 0$). Data from [601]

The term k^2 with curvature D (for the exciton polariton $D = \hbar/(M\,\omega_T)$) plays a role in particular when $\omega_T^2 - \omega^2 = 0$. For $\mathbf{k} \neq 0$ even a cubic material is anisotropic. The dimensionless curvature $\hat{D} = Dk'^2$ should fulfill $\hat{D} = \hbar/(Mc) \ll 1$ in order to make k^4 terms unimportant. For exciton polaritons[7] typically $\hat{D} = \hbar\omega_T/(m\,c^2) \approx 2 \times 10^{-5}$ for $\hbar\omega_T = 1$ eV and $m^* = 0.1$.

From (9.35) together with (9.36) two solutions result:

$$2\omega^2 = c^2k^2 + (1 + \beta + Dk^2)\omega_0^2 \pm \left[-4c^2k^2(1 + Dk^2)\omega_0^2 + (c^2k^2 + (1 + \beta + Dk^2)\omega_0^2)^2\right]^{1/2} . \tag{9.37}$$

The two branches are shown schematically in Fig. 9.21a. Depending on the k value they have a photonic (linear dispersion) or excitonic (quadratic

[7] The dependence of the optical-phonon energies on k is typically too small to make spatial dispersion effects important. According to (5.19) $\hat{D} = -(a_0\omega_{TO}/4c)^2 \approx 4 \times 10^{-11}$ for typical material parameters (lattice constant $a_0 = 0.5$ nm, TO phonon frequency $\omega_{TO} = 15$ THz).

dispersion) character. The anticrossing behavior at $k' \approx \omega_{\rm T}/c$ (for $\hbar\omega_{\rm T} = 1\,{\rm eV}$ $k' \approx 0.5 \times 10^{-5}\,{\rm cm}^{-1}$) creates a bottleneck region in the lower polariton branch. This name stems from the small emission rate of acoustic phonons (i.e. cooling) in that region, as predicted in [602] and experimentally found, e.g. in CdS [603]. The polaritons decay into a photon when they hit the surface. The effect of the oscillator strength of the dispersion is shown in Fig. 9.22 for two-exciton resonance. In the case of several excitons (9.36) reads

$$\epsilon(\omega) = \epsilon_{\rm b} \left[1 + \sum_{i=1}^{n} \frac{\beta_i}{1 - (\omega^2/\omega_{0,i})^2 + D_i\, k^2} \right] . \tag{9.38}$$

For $k = 0$ either $\omega = 0$ (lower polariton branch) or $\epsilon(\omega_{\rm L}) = 0$. For the latter we find from (9.36)

$$\omega_{\rm L} = \sqrt{1+\beta}\,\omega_{\rm T} . \tag{9.39}$$

Therefore, the energy splitting $\Delta E_{\rm LT}$, mostly denoted as $\Delta_{\rm LT}$, between the L- and T-exciton energy given by

$$\Delta E_{\rm LT} = \hbar(\omega_{\rm L} - \omega_{\rm T}) = \left[\sqrt{1+\beta} - 1\right] \hbar\omega_{\rm T} \approx \frac{1}{2}\,\beta\,\hbar\omega_{\rm T} \tag{9.40}$$

is proportional to the exciton oscillator strength (for experimental values see Table 9.5). We note that if (D.9) is used for the dielectric function, β in (9.40) needs to be replaced by $\beta/\epsilon_{\rm b}$.

The effect of spatial dispersion on the reflection at the fundamental exciton resonance is depicted in Fig. 9.21b. For non-normal incidence an additional feature due to the longitudinal wave is observed for p-polarization [601].

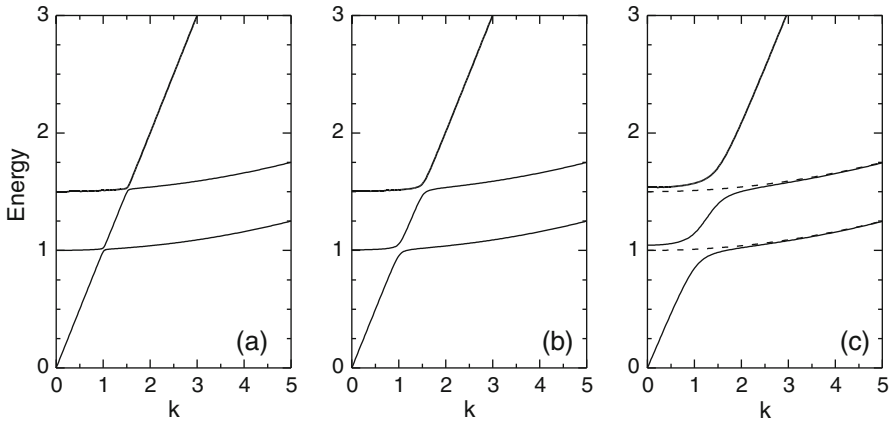

Fig. 9.22. Schematic polariton dispersion for a two-exciton resonance (curvature of exciton dispersion greatly exaggerated, $\hat{D} = 10^{-2}$) at $\omega_{{\rm T},1} = 1$ and $\omega_{{\rm T},2} = 1.5$ for three different oscillator strengths (**a**) $f = 10^{-3}$, (**b**) $f = 10^{-2}$, (**c**) $f = 10^{-1}$. The *dashed lines* in (**c**) represent the pure exciton dispersions

Table 9.5. Exciton energy (low temperature), LT splitting and exciton polariton oscillator strength for various semiconductors. Values for ZnO from [606], values for GaAs from [607], all other values from [608]

		CdS A	CdS B	ZnO A	ZnO B	ZnSe	GaN A	GaN B	GaAs
$\hbar\omega_T$	(eV)	2.5528	2.5681	3.3776	3.3856	2.8019	3.4771	3.4816	1.5153
Δ_{LT}	(meV)	2.2	1.4	1.45	5	1.45	1.06	0.94	0.08
β	(10^{-3})	1.7	1.1	0.9	3.0	1.0	0.6	0.5	0.11

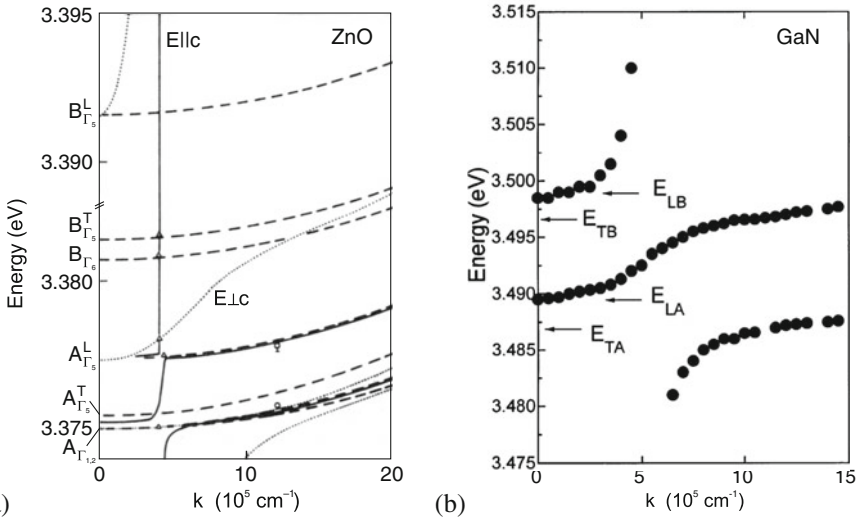

Fig. 9.23. (**a**) Exciton polariton dispersion ($\mathbf{k} \perp c$) of ZnO with experimental data ($T = 1.8\,\mathrm{K}$). *Solid* (*dotted*) *lines* are for polaritons with $\mathbf{E} \parallel c$ ($\mathbf{E} \perp c$). The *dashed lines* refer to excitons. Adapted from [609]. (**b**) Exciton polariton dispersion ($T = 2\,\mathrm{K}$) in GaN (on sapphire) for $\mathbf{E} \perp c$. Reprinted from [610], ©1998, with permission from Elsevier, originally in [611]

For a detailed discussion additional effects due to anisotropy in wurtzite crystals, an exciton free layer at the semiconductor surface, additional boundary conditions and damping need to be considered [604, 605]. The polariton dispersions of ZnO and GaN are shown in Fig. 9.23.

9.5.10 Bound-Exciton Absorption

Excitons can localize at impurities or inhomogeneities. Such excitons are called *bound excitons*. Here, the absorption due to such complexes is discussed. The recombination is discussed in Sect. 10.3.2. In GaP:N excitons are bound to isoelectronic N impurities (substituting P), resulting in the 'A'

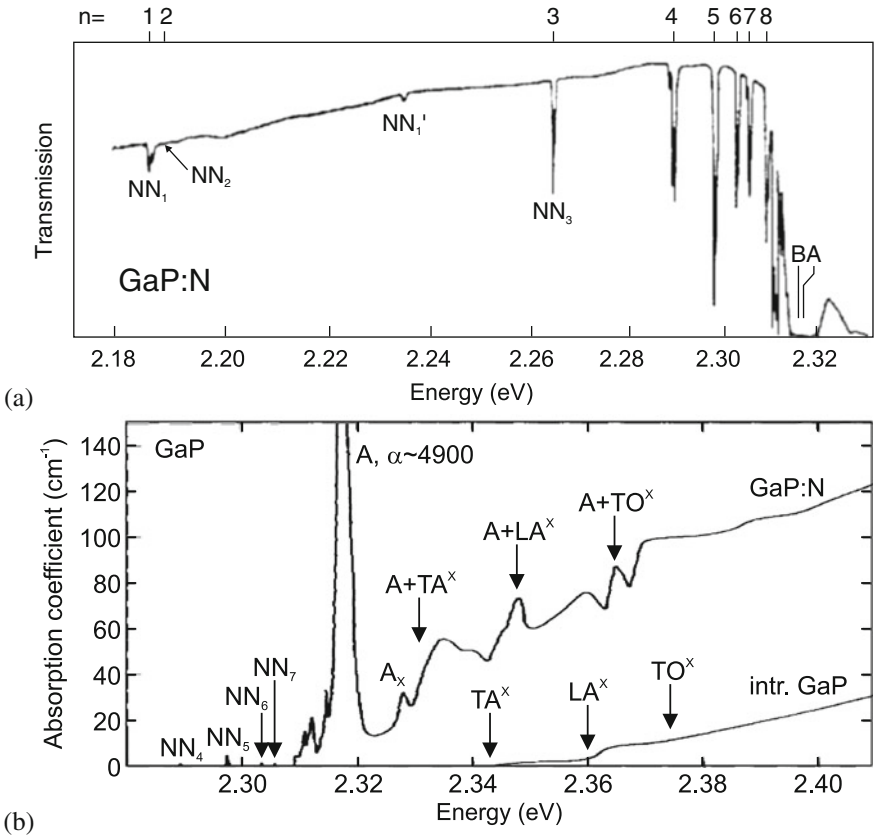

Fig. 9.24. (**a**) Transmission spectrum of GaP:N with a nitrogen concentration of about $10^{19}\,\mathrm{cm}^{-3}$ at 1.6 K (thickness: 1.1 mm). n is indicated for the first eight transitions due to excitons bound to nitrogen pairs. NN_n' indicate phonon replica. The 'A' line denotes the position of the transition due to excitons bound to a single nitrogen atom (observable for samples with low N doping). The 'B' line is forbidden and due to the $J = 2$ exciton. Adapted from [490]. (**b**) Absorption spectra of N-doped ($N_\mathrm{N} = 7 \times 10^{18}\,\mathrm{cm}^{-3}$) and intrinsic GaP ($T = 2\,\mathrm{K}$). Adapted from [484]

line at 2.3171 eV (at $T = 4.2\,\mathrm{K}$). The absorption due to A excitons is well resolved in the spectrum of Fig. 9.24b. At sufficiently high nitrogen doping, there exist nitrogen pairs, i.e. a complex where a nitrogen impurity has a second nitrogen impurity in the vicinity. The pairs are labeled NN_n. It was believed that the second nitrogen atom is in the n-th shell around the first one. However, the proper level assignment is probably different in the view of modern theory [369]. Also clusters with more than two nitrogen atoms may exist. NN_1 is a prominent level and relates to a N–Ga–N complex having 12 equivalent sites for the second N atom on the next neighbor anion site. The

Table 9.6. Index of nitrogen pairs NN_n and energy separation ΔE of bound-exciton transitions from the free-exciton line for $n = 1 \ldots 10$ and the 'A' line

n	1	2	3	4	5	6	7	8	9	10	∞ (A)
ΔE (meV)	143	138	64	39	31	25	22	20	18	17	11

transitions due to excitons bound to NN_n, as shown in Fig. 9.24a, give a series of lines (see Table 9.6) that fulfill $\lim_{n\to\infty} NN_n = A$. Although GaP has an indirect band structure, the absorption coefficient of N-related transitions is large, about $10^5\,cm^{-1}$ for a nitrogen doping level of $10^{19}\,cm^{-3}$.[8] This is due to the fact that the electron spatially localized at the nitrogen isoelectronic trap (Sect. 7.7.9) has a sizeable $k = 0$-component of its wave-function (Fig. 7.36), leading to a large transition probability with Γ-point holes with an oscillator strength of 0.09 [612].

9.5.11 Biexcitons

Similar to two hydrogen atoms forming a hydrogen molecule, two excitons can also form a bound complex, the biexciton involving two electrons and two holes. The biexciton binding energy is defined as

$$E_{XX}^{b} = 2\,E_X - E_{XX}\ . \tag{9.41}$$

Biexcitons are binding in bulk material. Accordingly, the biexciton recombination or absorption occurs at lower energy than that of the exciton. Values of the biexciton binding energy are listed in Table 9.3 for various semiconductors. The ratio of biexciton and exciton binding energies is fairly constant about 0.2. In semiconductors with small exciton binding energy, such as GaAs, biexcitons are hard to observe in bulk material but show up in heterostructures that provide additional carrier confinement (see also Sect. 13.3.4). While the exciton density increases linearly with external excitation, the density of biexcitons increases quadratically.

9.5.12 Trions

The complexes 'eeh' and 'ehh' are called trions. Also, the notation X^- and X^+ is common. X^- is typically stable in bulk material but hard to observe. In quantum wells or dots, trions are easier to observe. In quantum dots excitons with higher charge, e.g. X^{2-}, have also been observed (see Fig. 13.34).

[8] Also the recombination (Sect. 10.3.2) is efficient and allows green GaP:N and yellow GaAsP:N light emitting diodes.

9.5.13 Burstein–Moss Shift

In the discussion so far it has been assumed that all target states in the conduction band are empty. In the presence of free carriers the absorption is modified by the

- change of the distribution function
- many-body effects (band gap renormalization)

The latter is discussed in the next section. For a degenerate electron distribution all states close to the conduction-band edge are populated. Thus a transition from the valence band cannot take place into such states. This shift of the absorption edge to higher energies is called the Burstein–Moss shift [613, 614].

k-conserving optical transitions between parabolic hole and electron bands have the dependence

$$E = E_\mathrm{g} + \frac{\hbar^2 k^2}{2m_\mathrm{e}^*} + \frac{\hbar^2 k^2}{2m_\mathrm{h}^*} = E_\mathrm{g} + \frac{\hbar^2 k^2}{2m_\mathrm{r}} \,, \tag{9.42}$$

where m_r is the reduced mass of electron and hole. About $4kT$ below the Fermi level all levels in the conduction band are populated (Fig. 9.25). Thus the k value at which the absorption starts is given as

$$\hat{k} = \sqrt{\frac{2m_\mathrm{r}}{\hbar^2}\left(E_\mathrm{F} - E - 4kT\right)} \,. \tag{9.43}$$

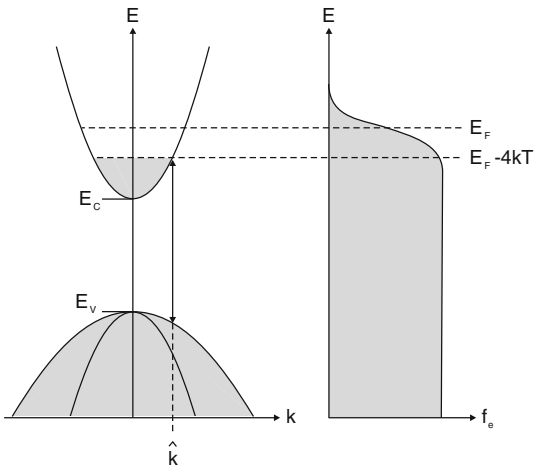

Fig. 9.25. Principle of Burstein–Moss shift. *Left panel*: Schematic band structure with completely filled electron states shown in *grey*. The k-vector for the lowest photon energy optical absorption process is indicated as $\hat{k}$. *Right panel*: Electron distribution function for a degenerate electron gas with Fermi level in the conduction band

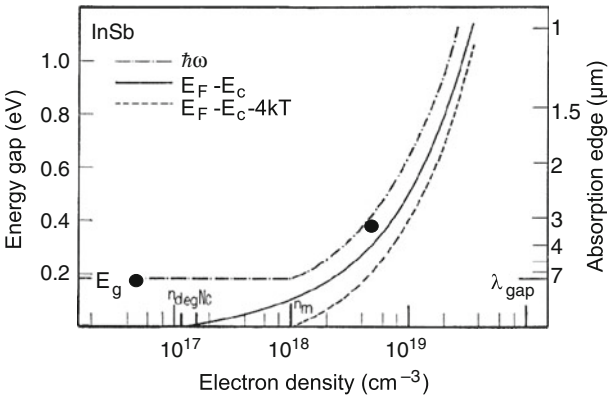

Fig. 9.26. Burstein–Moss effect at InSb ($E_\mathrm{g} = 0.18\,\mathrm{eV}$) at room temperature. Theoretical dependence and data points for intrinsic InSb and $5 \times 10^{18}\,\mathrm{cm}^{-3}$ n-type. Data from [613]

Besides the energy shift in the conduction band, the corresponding energy shift in the valence band $\hbar k^2/(2m_\mathrm{h})$ must be considered. Thus, the Burstein–Moss shift of the absorption edge is

$$\Delta E = \hbar\omega - E_\mathrm{g} = (E_\mathrm{F} - 4kT - E_\mathrm{C}) \left(1 + \frac{m_\mathrm{e}}{m_\mathrm{h}}\right) . \tag{9.44}$$

The relation between n and the Fermi level is given by (7.8). If $E_\mathrm{F} - E_\mathrm{C} \gg kT$ the Fermi integral can be approximated by $\frac{2}{\sqrt{\pi}} \left(\frac{E_\mathrm{F}-E_\mathrm{C}}{kT}\right)^{3/2}$. Using (7.10) for N_C, the Burstein–Moss shift can be written for this case as

$$\Delta E = n^{2/3} \frac{h^2}{8m_\mathrm{e}} \left(\frac{3}{\pi}\right)^{2/3} \left(1 + \frac{m_\mathrm{e}}{m_\mathrm{h}}\right) \approx 0.97 \frac{h^2}{8m_\mathrm{r}} n^{2/3} . \tag{9.45}$$

Originally, the Burstein–Moss shift was evoked to explain the absorption shift in InSb with varying carrier concentration (Fig. 9.26).

9.5.14 Band Gap Renormalization

The band structure theory has been developed so far for small carrier densities. If the carrier density is large the interaction of free carriers has to be considered. The first step was exciton formation. However, at high temperatures (ionization) and at large carrier density (screening) the exciton is not stable. Exchange and correlation energy leads to a decrease of the optical absorption edge that is called *band gap renormalization* (BGR).

An effect due to significant carrier density is to be expected when the density is of the order of the exciton volume, i.e. $n \sim a_\mathrm{B}^{-3}$. For $a_\mathrm{B} \sim 15\,\mathrm{nm}$ (GaAs) this means $n \sim 3 \times 10^{17}\mathrm{cm}^{-3}$. The dimensionless radius r_s is defined via

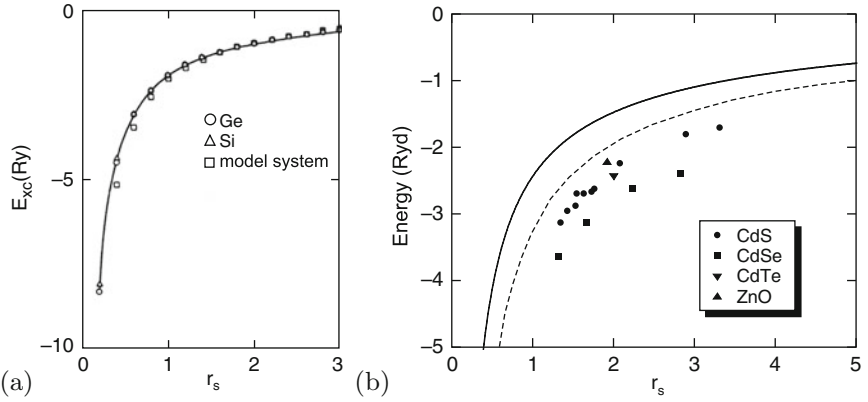

Fig. 9.27. (**a**) Theoretical exchange and correlation energies in units of the exciton Rydberg energy as a function of the dimensionless variable r_s for Ge, Si and a model system (with one isotropic conduction and valence band each). The *solid line* is a fit according to (9.47). Adapted from [615]. (**b**) Band gap renormalization in terms of the excitonic Rydberg for various II–VI semiconductors. *Solid line* is the relation according to (9.47), *dashed line* is the dependence predicted in [619] for $T = 30\,\mathrm{K}$. Data are compiled in [620]

$$\frac{4\pi}{3}\, r_s^3 = \frac{1}{n\, a_B^3}\ . \tag{9.46}$$

The sum of exchange and correlation energies E_{xc} is found to be mostly independent of material parameters [615] (Fig. 9.27a) and follows the form

$$E_{xc} = \frac{a + b\, r_s}{c + d\, r_s + r_s^2}\ , \tag{9.47}$$

with $a = -4.8316$, $b = -5.0879$, $c = 0.0152$ and $d = 3.0426$. Thus the density dependence of the band gap at small carrier density is $\propto n^{1/3}$. Experimental data for a number of II–VI semiconductors roughly follow such a dependence (Fig. 9.27b).

In Fig. 9.28, a theoretical calculation of the absorption spectrum of bulk GaAs for various carrier densities (n=p) [616] is shown. With increasing density, the excitonic resonance broadens and vanishes. The shape approaches the electron–hole plasma shape. The absorption edge shifts to smaller energies. At high carrier density, the absorption becomes negative in a spectral range before absorption sets in. In this spectral region, the material exhibits gain and an incoming light wave is amplified (cmp. Sect. 10.2.6).

9.5.15 Electron–Hole Droplets

At low temperature and high density, electron–hole pairs in Ge and Si can undergo a phase transition into a liquid state. This electron–hole liquid (EHL)

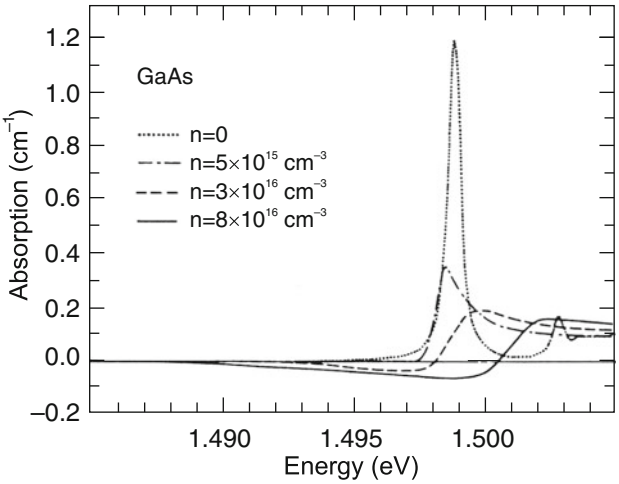

Fig. 9.28. Absorption of GaAs (low temperature, $T = 10\,\mathrm{K}$) as a function of the electron–hole density n (theory). Adapted from [616]

was suggested in [617] and is a Fermi liquid exhibiting the high conductivity of a metal and the surface and density of a liquid. The condensation is due to exchange interaction and correlation. The formation is fostered by the band structure of Ge [618] and the long lifetime of carriers in the indirect band structure. In unstressed Ge typically a cloud of electron–hole droplets with diameter in the µm range exists. The phase diagram is shown in Fig. 9.29a. In suitably stressed Ge electron–hole droplets with several hundred µm diameter form around the point of maximum shear strain in inhomogeneously strained crystals, as shown in Fig. 9.29b. The pair density in such a liquid is of the order of $10^{17}\,\mathrm{cm}^{-3}$.

We note that the metallic EHL state hinders observation of the Bose–Einstein condensation (BEC) of (bosonic) excitons. The light-exciton mass offers a high condensation temperature in the 1 K range (compared to the mK range for atoms). Recent experiments with spatially indirect excitons in coupled quantum wells lead towards BEC [624, 625]. A sufficiently long lifetime ensures cooling of the excitons close to the lattice temperature. Another potential candidate for BEC are long-living excitons (ms-range) in Cu_2O [626]. The condensation of polaritons (cf. Sect. 9.5.9) in microcavities to well-defined regions of **k**-space has been discussed in [627] and compared to bosonic condensation in bulk.

9.5.16 Two-Photon Absorption

So far, only absorption processes that involve one photon have been considered. The attenuation of the intensity I of a light beam (of frequency ω_0) along the z direction can be written as

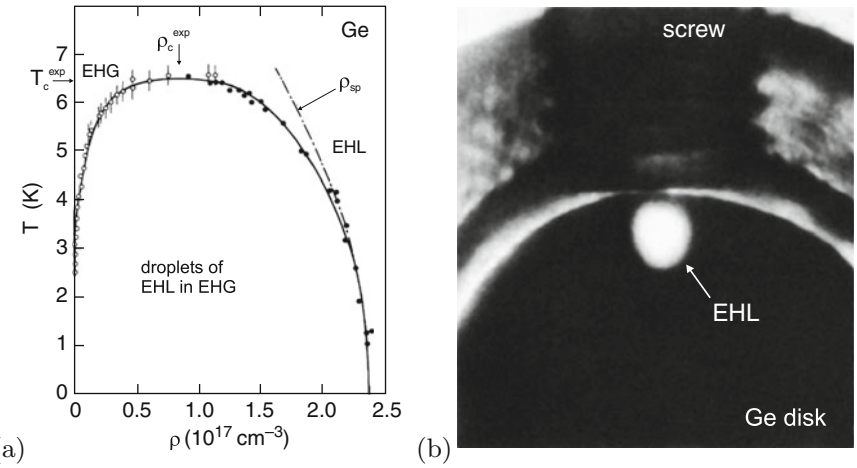

Fig. 9.29. (**a**) Temperature–density phase diagram of electrons and holes in Ge. The regions of electron–hole gas (EHG) and liquid (EHL) and the droplet phase are labeled. *Solid line* is theoretical calculation, *symbols* are experimental data from [621]. The *dash-dotted line* denoted ρ_{sp} is the experimentally obtained temperature dependence of the liquid density due to single-particle excitations. ρ_c^{exp} and T_c^{exp} denote the experimental critical density and temperature, respectively. Adapted from [622]. (**b**) Photographic image of radiative recombination (at 1.75 µm wavelength) from a 300-µm diameter droplet of electron–hole liquid (EHL) in a stressed (001) Ge disk (diameter 4 mm, thickness 1.8 mm) at $T = 2$ K. The stress is applied from the top by a nylon screw along a ⟨110⟩ direction. Adapted from [623], reprinted with permission, ©1977 APS

$$\frac{\mathrm{d}I}{\mathrm{d}z} = -\alpha\, I - \beta\, I^2 \,, \tag{9.48}$$

where α is due to the (linear) absorption coefficient (and possibly scattering) and β is the two-photon absorption coefficient. A two-photon process can occur in two steps, e.g. via a midgap level, which is not considered any further here. Here, we consider two-photon absorption (TPA) via the population of a state at $2\hbar\omega_0$ higher energy than the initial state with a nonlinear optical process. The TPA coefficient is related to the nonlinear third-order electric dipole susceptibility tensor [629] χ_{ijkl}. Within the two-band approximation theory predicts [630]

$$\beta \propto (2\hbar\omega_0 - E_g)^{3/2} \,. \tag{9.49}$$

The exponent 3/2 is indeed found experimentally, as shown in Fig. 9.30 for GaAs. The strength of absorption depends on the relative orientation of the light polarization with respect to the main crystallographic directions, e.g. TPA for polarization along ⟨110⟩ is about 20% larger than for the ⟨100⟩ orientation.

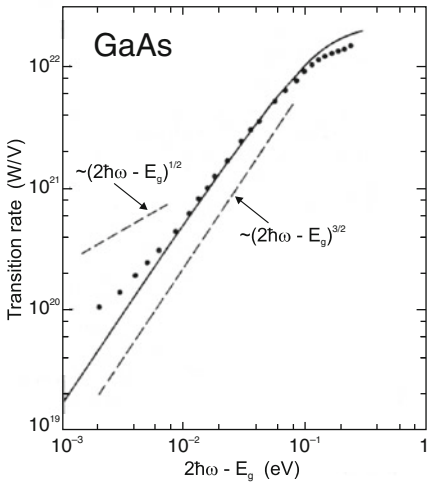

Fig. 9.30. Experimental (*dots*) two-photon absorption of GaAs ($T = 4\,\mathrm{K}$) as a function of the difference of the double-photon energy $2\hbar\omega$ from the GaAs band edge E_g. The *solid line* is a theoretical calculation, the *dashed lines* represent slopes with exponent 1/2 and 3/2, respectively. Adapted from [628]

9.6 Impurity Absorption

Charge carriers bound to shallow impurities exhibit a hydrogen-like term scheme

$$E_n = \frac{m^*}{m_0}\frac{1}{\epsilon_\mathrm{r}^2}\frac{1}{n^2} \times 13.6\,\mathrm{eV}\ , \tag{9.50}$$

with the ionization limit E_∞ being the conduction (valence) band edge for donors (acceptors), respectively. They can be excited by light to the nearest band edge. Such absorption is typically in the FIR region and can be used for photodetectors in this wavelength regime. The optical absorption cross section of impurity absorption can be related to the carrier capture cross section [395, 396].

The actual transition energies can deviate from (9.50) due to deviation of the potential close to the impurity from the pure Coulomb potential. Such an effect is known as the chemical shift or central cell correction (cf. Sect. 7.5.5) and is characteristic of the particular impurity. In GaAs such shifts are small ($\sim 100\,\mu\mathrm{eV}$) [632].

The term scheme for P in Si is shown in Fig. 9.31a. The ground state (1s) is split because of a reduction of the tetrahedral symmetry due to intervalley coupling. The anisotropic mass at the X-valley in Si causes the p states (and states with higher orbital momentum) to split into p_0 and $\mathrm{p}_\pm$ states. Such an effect is absent in a direct semiconductor with an isotropic conduction-band minimum such as GaAs (Fig. 9.32). Optical transitions between the

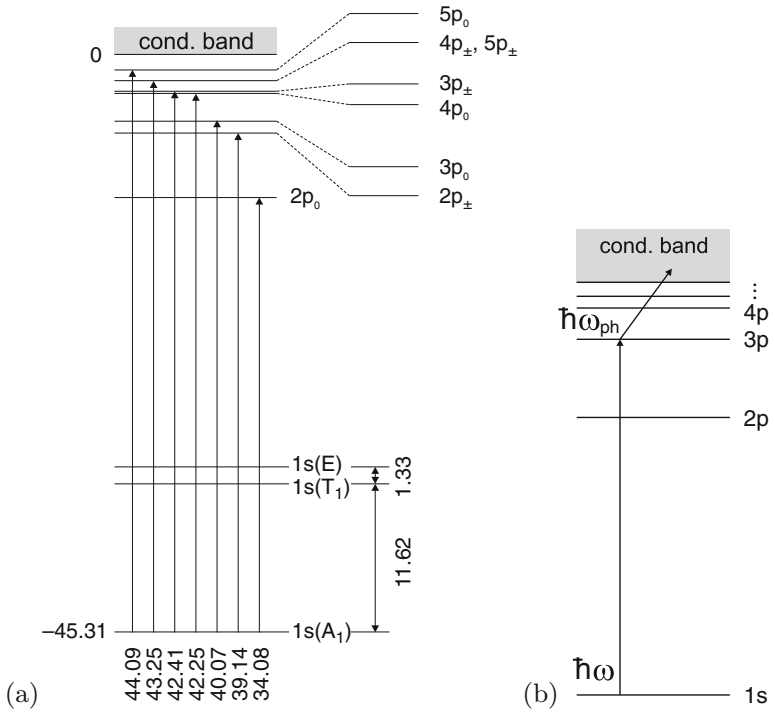

Fig. 9.31. (**a**) Term scheme of phosphorus donor in silicon, all energies in meV. After [631]. (**b**) Schematic sequence for photothermal ionization, here absorption of a photon with $\hbar\omega = E_{3p} - E_{1s}$ and subsequent absorption of a phonon with energy $\hbar\omega_{ph} \geq E_{\infty} - E_{3p}$

1s and various p states can be directly observed in absorption, e.g. for Si:P in [634]. These transitions are also observed in photoconductivity because the missing energy to the ionization into the continuum is supplied by a phonon at finite temperature (photothermal ionization) (Fig. 9.31b) [631]. The splitting of the 2p transition in Fig. 9.32a is the chemical shift due to different donors incorporated in the GaAs (Si, Sn, and Pb). Peak broadening is mostly due to Stark broadening due to neighboring charged impurities. The application of a magnetic field induces Zeeman-like splittings and increases the sharpness of the peaks. The peak width can be further increased by illuminating the sample with light having a higher energy than the band gap. The additional charge carriers neutralize charged impurities and allow higher resolution (Fig. 9.32b).

In Fig. 9.33 absorption spectra of highly doped n-type GaAs are shown. For doping concentrations larger than the critical concentration of $\sim 1 \times 10^{16}\,\mathrm{cm}^{-3}$ (cf. Table 7.6) significant broadening is observed due to the formation of an impurity band.

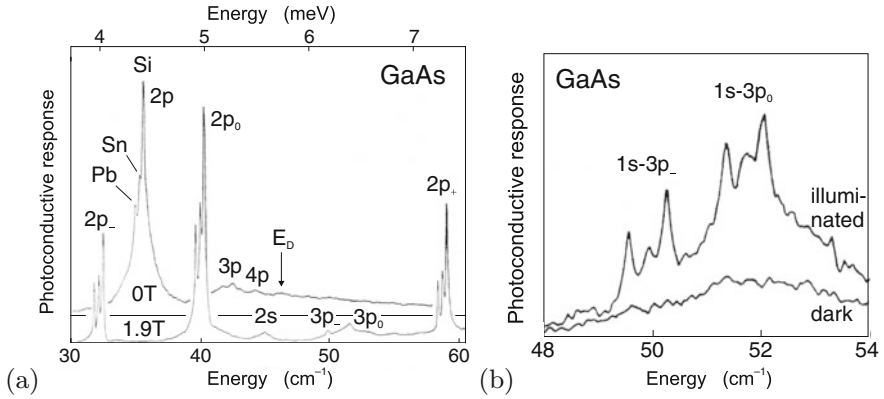

Fig. 9.32. (**a**) Far-infrared photoconductivity response (Lyman-type s→p series) of not intentionally doped GaAs with residual donors Pb, Sn, and Si, $N_A = 2.6 \times 10^{13}\,cm^{-3}$, $N_D - N_A = 8 \times 10^{12}\,cm^{-3}$. The *upper* (*lower*) curve is for a magnetic field of 0 (1.9) T. Measurement temperature is 4.2 K. (**b**) Photoconductive response of a (different) GaAs sample with the same impurities ($N_D = 1 \times 10^{13}\,cm^{-3}$) with (*upper curve*) and without (*lower curve*) illumination with above-bandgap light ($B = 1.9$ T, $T = 4.2$ K). Adapted from [633]

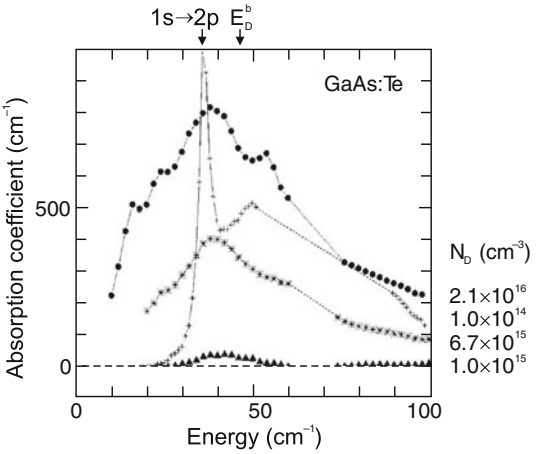

Fig. 9.33. Low-temperature ($T = 1.35$ K) absorption spectra of highly doped n-type GaAs:Te with doping concentrations as labeled (*circles*: $N_D = 2.1 \times 10^{16}\,cm^{-3}$, *stars*: 6.7×10^{14}, *triangles*: 1.0×10^{15}). A sharp photoconductivity spectrum (in arbitrary units) from low-doped GaAs:Te (*crosses*, $N_D = 1.0 \times 10^{14}\,cm^{-3}$) is shown for comparison (cf. Fig. 9.32a). The energy of the 1s→2p transition and the donor binding energy (onset of continuum absorption) are indicated. Adapted from [636]

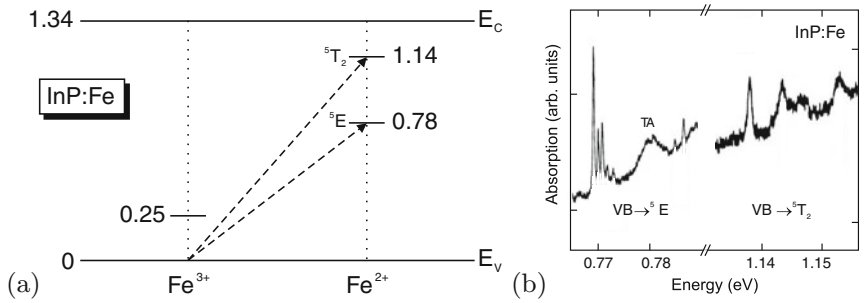

Fig. 9.34. (**a**) Schematic band diagram of InP with levels of Fe impurities in the 3+ and 2+ charge states at low temperature. All energies are given in eV. The *arrows* denote the optical transition of a valence-band electron to the Fe center, $Fe^{3+} + \hbar\omega \rightarrow Fe^{2+} + h$. (**b**) Calorimetric absorption spectra (at $T = 1.3\,\mathrm{K}$) of InP:Fe, [Fe]=$5 \times 10^{16}\,\mathrm{cm}^{-3}$. Part (**b**) adapted from [476]

The absorption of deep levels is typically in the infrared. In Fig. 9.34a the possible optical absorption processes involving the Fe levels in InP (cf. Sect 7.7.8) during the charge transfer $Fe^{3+} \rightarrow Fe^{2+}$ are shown. These transitions and their fine structure (Fig. 9.34b) have been observed in calorimetric absorption spectroscopy (CAS) experiments [476].

In Fig. 9.35 the photoconductivity of Si:Mg is shown. The sharp peaks are due to transitions of interstitial, singly ionized Mg, Mg_i^+ [635]. Mg in Si is a double donor [449] (see Sect. 7.7.2). Above the ionization limit of about 256 meV, the peaks are replicated, shifted by the LO phonon energy of 59.1 meV. However, now they rather appear as dips. This behavior is typical for a discrete state interacting with a continuum, also called Fano resonance [637, 638] with its characteristic lineshape, going *below* the continuum level.

9.7 Free-Carrier Absorption

A time-dependent electric field accelerates the charge carriers. The excess energy is subsequently transferred to the lattice via scattering with phonons. A review of the effect of free carriers on optical properties can be found in [639]. In the relaxation-time approximation energy is relaxed with a time constant τ. Thus energy is absorbed from the electromagnetic wave and dissipated.

The complex conductivity (8.48) is given by

$$\sigma^* = \sigma_\mathrm{r} + \mathrm{i}\sigma_\mathrm{i} = \frac{ne^2\tau}{m^*}\left(\frac{1}{1+\omega^2\tau^2} + \mathrm{i}\frac{\omega\tau}{1+\omega^2\tau^2}\right) . \qquad (9.51)$$

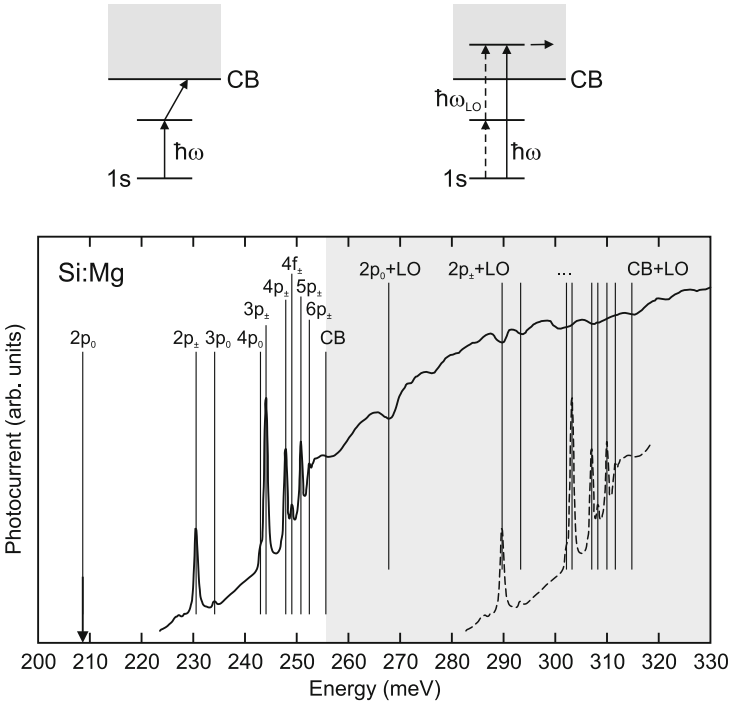

Fig. 9.35. Photocurrent spectrum of Si:Mg. Transitions are due to Mg_i^+ from its 1s state to excited states as labeled and indicated by *vertical lines*. CB denotes the conduction band edge (ionization limit). Above the CB edge (*shaded area*) phonon-assisted absorption occurs (Fano resonances). For comparison the absorption spectrum below CB is shown shifted by the phonon energy (*dashed line*). Above the plot, the transition mechanisms (photothermal ionization and Fano resonance) are schematically shown. Adapted from [635]

We note that a static magnetic field introduces birefringence as discussed in more detail in Sect. 12.2.1. The wave equation for the electric field is

$$\nabla^2 \mathbf{E} = \epsilon\mu_0 \ddot{\mathbf{E}} + \sigma\mu_0 \dot{\mathbf{E}} \,. \tag{9.52}$$

For a plane wave $\propto \exp[\mathrm{i}(\mathbf{kr} - \omega t)]$ the wavevector obeys

$$k = \frac{\omega}{c}\sqrt{\epsilon_\mathrm{r} + \mathrm{i}\frac{\sigma^*}{\epsilon_0\omega}} \,, \tag{9.53}$$

where $c = (\epsilon_0\mu_0)^{-1/2}$ is the velocity of light in vacuum, ϵ_r is the background dielectric constant (for large ω).

The part $\boldsymbol{\epsilon}_\mathrm{FC}$ of the dielectric tensor due to free carriers is

$$\boldsymbol{\epsilon}_\mathrm{FC} = \frac{\mathrm{i}}{\epsilon_0\omega}\boldsymbol{\sigma}^* \,. \tag{9.54}$$

The complex index of refraction is

$$n^* = n_\mathrm{r} + \mathrm{i}\kappa = \sqrt{\epsilon_\mathrm{r} + \mathrm{i}\frac{\sigma^*}{\epsilon_0\omega}} \,. \tag{9.55}$$

Taking the square of this equation yields

$$n_\mathrm{r}^2 - \kappa^2 = \epsilon_\mathrm{r} + \mathrm{i}\,\frac{\sigma_\mathrm{i}}{\epsilon_0\omega} = \epsilon_\mathrm{r} - \frac{ne^2}{\epsilon_0 m^*}\,\frac{\tau^2}{1+\omega^2\tau^2} \tag{9.56a}$$

$$2n_\mathrm{r}\,\kappa = \frac{\sigma_\mathrm{r}}{\epsilon_0\omega} = \frac{ne^2}{\epsilon_0\omega m^*}\,\frac{\tau}{1+\omega^2\tau^2} \,. \tag{9.56b}$$

The absorption coefficient is related to κ by (9.10). For the case of higher frequencies, i.e. $\omega\tau \gg 1$, the absorption is

$$\alpha = \frac{n\,e^2}{\epsilon_0 c n_\mathrm{r} m^* \tau}\,\frac{1}{\omega^2} \,. \tag{9.57}$$

The absorption decreases with increasing frequency. For semiconductors it is particularly important in the mid- and far-infrared regions when carriers are present due to doping or thermal excitation. In Fig. 9.36a absorption spectra of n-type Ge for various doping concentrations are shown. The absorption coefficient in the transparency regime varies proportionally to $\lambda^2 \propto \omega^{-2}$ as predicted in (9.57). A more detailed discussion of the energy dependence of free carrier absorption can be found in [640]. In Fig. 9.36b the absorption coefficient due to free carrier absorption at fixed wavelength is shown as a function of dopant concentration.[9] The slope is slightly overlinear, indicating a weak dependence $\tau(n)$.

The index of refraction is given by (also for $\omega\tau \gg 1$)

$$n_\mathrm{r}^2 = \epsilon_\mathrm{r} - \frac{ne^2}{\epsilon_0 m^*\omega^2} + \kappa^2 = \epsilon_\mathrm{r}\left[1 - \left(\frac{\omega_\mathrm{p}}{\omega}\right)^2\right] + \frac{\epsilon_\mathrm{r}^2}{4n_\mathrm{r}^2}\left(\frac{\omega_\mathrm{p}}{\omega}\right)^4 \frac{1}{\omega^2\tau^2} \tag{9.58}$$

$$\approx \epsilon_\mathrm{r}\left[1 - \left(\frac{\omega_\mathrm{p}}{\omega}\right)^2\right] \,,$$

where

$$\omega_\mathrm{p} = \sqrt{\frac{ne^2}{\epsilon_\mathrm{r}\epsilon_0 m^*}} \tag{9.59}$$

is the plasma frequency. The approximation is valid for small absorption and when $(\omega\tau)^{-2}$ can be neglected. A graphical representation is given in Fig. 9.37a. For coupling to electromagnetic waves (still $\omega\tau \gg 1$)

[9] Even at low temperature, $n \approx N_\mathrm{D}$ since $N_\mathrm{D} \gg N_\mathrm{c}$ (cf. [421] and Sect. 7.5.6).

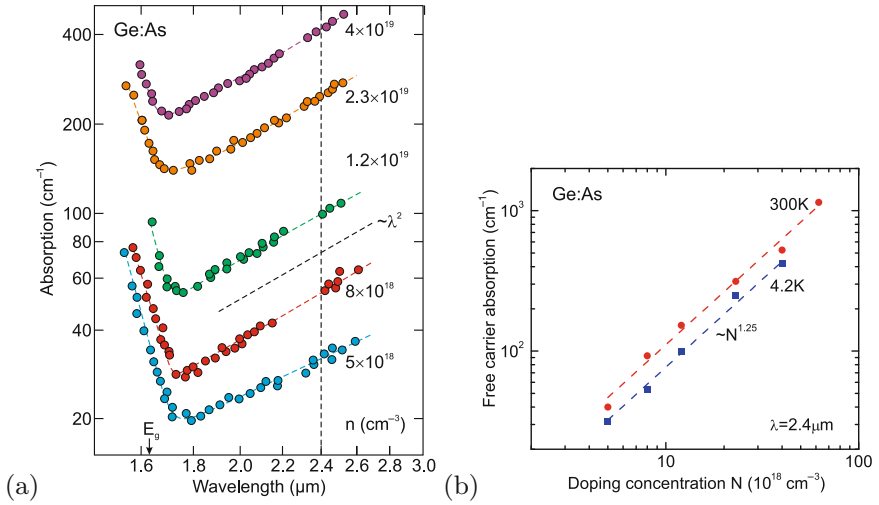

Fig. 9.36. (**a**) Optical absorption spectra (at $T = 4.2\,\mathrm{K}$) of n-type Ge for various As dopant concentrations as labeled. The *arrow* denotes the band edge of undoped Ge, the *vertical dashed line* the energy for which the free carrier absorption is measured in part (**b**). The inclined *dashed line* visualizes the slope $\propto \lambda^2$. *Curved dashed lines* are guides to the eye. Adapted from [577]. (**b**) Free carrier absorption at $\lambda = 2.4\,\mu\mathrm{m}$ as determined from part (**a**) of the figure (*blue squares*) as a function of As dopant concentration. Additionally data at 300 K (*red circles*) from the same samples are included [577]. The *dashed lines* visualizes the slope $\propto N_\mathrm{D}^{1.25}$

$$\epsilon(\omega) = \epsilon_\mathrm{r}\left[1 - \left(\frac{\omega_\mathrm{p}}{\omega}\right)^2\right] = \frac{c^2\,k^2}{\omega^2} \tag{9.60}$$

must be fulfilled. It follows that the dispersion relation in the presence of free carriers (Fig. 9.37b) is

$$\omega^2 = \omega_\mathrm{p}^2 + \frac{c^2\,k^2}{\epsilon_\mathrm{r}^2}\ . \tag{9.61}$$

For $\omega > \omega_\mathrm{p}$, $\epsilon > 0$, thus waves can propagate. For $\omega < \omega_\mathrm{p}$, however, the dielectric constant is negative, i.e. $\epsilon < 0$. For such frequencies waves are exponentially damped and cannot propagate or penetrate a layer. This effect can be used in a plasmon waveguide. The expected dependence of the plasmon wavelength on the carrier density $\lambda_\mathrm{p} = 2\pi c/\omega_\mathrm{p} \propto n^{-1/2}$ is depicted in Fig. 9.38 for GaAs. For semiconductors the plasmon frequency is in the mid-or far-infrared spectral region.[10]

[10] The much higher free-electron density in metals shifts the plasma frequency to the UV, explaining the reflectivity of metals in the visible and their UV transparency.

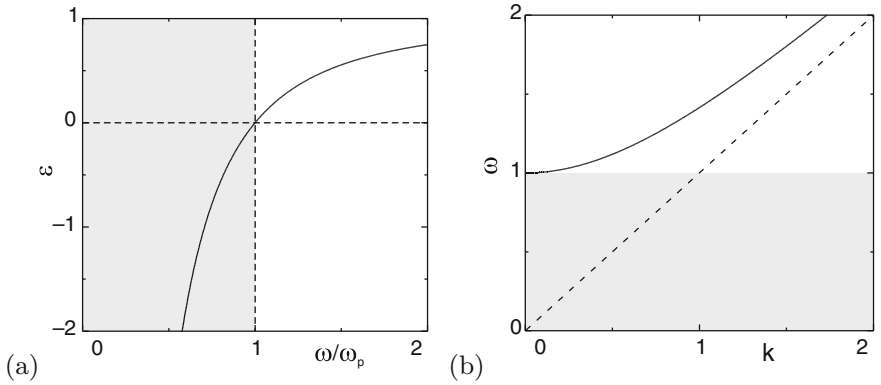

Fig. 9.37. (**a**) Dielectric constant for plasmon oscillations. *Shaded area* represents region of attenuation (negative ϵ). (**b**) Dispersion relation (k in units of ω_p/c, ω in units of ω_p) in the presence of free carriers (9.61, for $\epsilon_r = 1$). *Shaded area* represents forbidden frequency range for propagating solutions. *Dashed line* is photon dispersion $\omega = ck$

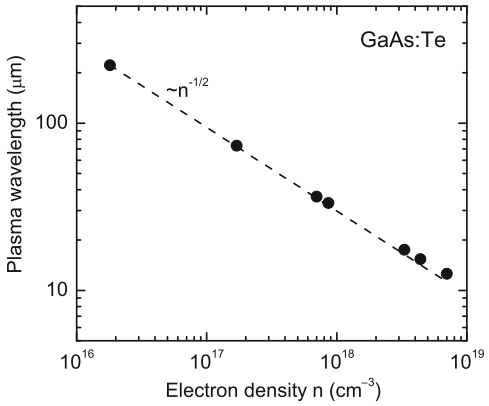

Fig. 9.38. Plasma wavelength λ_p for n-type GaAs with various electron concentrations due to different doping levels. *Filled circles*: experimental values, *dashed line*: $n^{-1/2}$ dependence; the deviation is due to nonparabolicity of the electron mass (cf. Fig. 9.42b). Data from [641]

9.8 Lattice Absorption

While there is no interaction of optical phonons and (infrared) light in Si and Ge due to crystal structure symmetry [642], strong effects are present for compound semiconductors. A review can be found in [643].

9.8.1 Dielectric Constant

The dielectric constant (with damping parameter Γ) in the vicinity of the optical phonon energies is given by (cf. (5.49))

$$\epsilon(\omega) = \epsilon(\infty) \left(\frac{\omega_{\mathrm{LO}}^2 - \omega^2 - \mathrm{i}\omega\Gamma}{\omega_{\mathrm{TO}}^2 - \omega^2 - \mathrm{i}\omega\Gamma} \right) . \tag{9.62}$$

The dispersion relation (without damping) can be written as

$$\epsilon(\omega) = \epsilon(\infty) + \frac{\epsilon(0) - \epsilon(\infty)}{1 - (\omega/\omega_{\mathrm{LO}})^2} = \epsilon(\infty) \left[1 + \frac{f}{1 - (\omega/\omega_{\mathrm{LO}})^2} \right] . \tag{9.63}$$

Thus the oscillator strength (compare with (D.10)) is $f = \frac{\epsilon(0)-\epsilon(\infty)}{\epsilon(\infty)}$. With the LST relation (5.48) the oscillator strength is

$$f = \frac{\omega_{\mathrm{LO}}^2 - \omega_{\mathrm{TO}}^2}{\omega_{\mathrm{TO}}^2} \approx 2 \frac{\omega_{\mathrm{LO}} - \omega_{\mathrm{TO}}}{\omega_{\mathrm{TO}}} , \tag{9.64}$$

and thus proportional to the splitting $\Delta_{\mathrm{LT}} = \omega_{\mathrm{LO}} - \omega_{\mathrm{TO}}$ between the longitudinal and transverse optical phonon frequency. The approximation in (9.64) is valid for $\Delta_{\mathrm{LT}} \ll \omega_{\mathrm{TO}}$.

The oscillator strength increases with the ionicity, i.e. the electronegativity difference of the atoms in the base (Fig. 9.39). Additionally, the oscillator strength depends on the reduced mass and the high-frequency polarizability; this can be seen, e.g., for the series of the Zn compounds that all have similar ionicity. For the series of the nitrides, the mass effect is small since the reduced mass is dominated by the light N mass.

9.8.2 Reststrahlenbande

The absorption of electromagnetic radiation by optical phonons is governed by the dielectric function that has been derived in (9.62). For small damping, i.e. $\Gamma \ll \Delta_{\mathrm{LT}}$, the dielectric constant is negative between ω_{TO} and ω_{LO}. From $\epsilon_{\mathrm{r}} = n_{\mathrm{r}}^2 - \kappa^2$ it follows that κ^2 is much larger than n_{r}^2. Therefore, the reflectance (9.9) will be close to 1. This energy range is the so-called *reststrahlenbande*. This term stems from multiple reflections in this wavelength regime that suppresses neighboring spectral regions and thus achieves a certain monochromatization in the far-infrared spectral region. Within the semiconductor the absorption is large in the reststrahlenbande (Fig. 9.40).

9.8.3 Polaritons

The coupled propagation of phonons and electromagnetic radiation is related to the equation (without phonon damping)

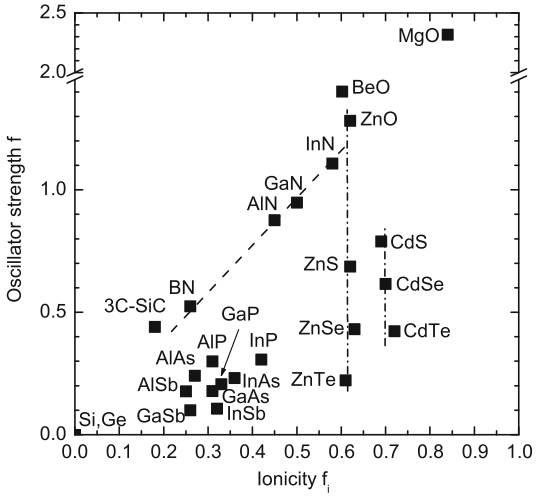

Fig. 9.39. Lattice absorption oscillator strength f from (9.64) for various elemental, III–V and II–VI semiconductors as a function of their ionicity f_i (cf. Table 2.1). *Dashed line* is linear dependence on ionicity for similar (reduced) mass, *dash-dotted lines* are guides to the eye for similar ionicity and varying mass

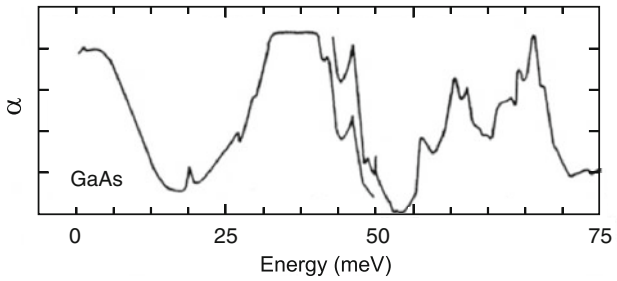

Fig. 9.40. Far-infrared absorption of GaAs. In the region around 35 meV is the reststrahlenbande with high absorption due to optical phonons. Adapted from [192], based on [644]

$$\epsilon(\omega) = \epsilon(\infty)\left(\frac{\omega_{\mathrm{LO}}^2 - \omega^2}{\omega_{\mathrm{TO}}^2 - \omega^2}\right) = \frac{c^2\,k^2}{\omega^2}\ . \tag{9.65}$$

There are two branches of propagating waves (real k):

$$\omega^2 = \frac{1}{2}\left(\omega_{\mathrm{LO}}^2 + \frac{c^2k^2}{\epsilon(\infty)}\right) \pm \sqrt{\frac{1}{4}\left(\omega_{\mathrm{LO}}^2 + \frac{c^2k^2}{\epsilon(\infty)}\right)^2 - \left(\frac{c^2k^2\omega_{\mathrm{TO}}^2}{\epsilon(\infty)}\right)^2}\ . \tag{9.66}$$

For $k = 0$ we find the solutions $\omega = \omega_{\mathrm{LO}}$ and $\omega = kc/\sqrt{\epsilon(0)}$. For large k we find $\omega = \omega_{\mathrm{TO}}$ and $\omega = kc/\sqrt{\epsilon(\infty)}$. These solutions are shown in Fig. 9.41.

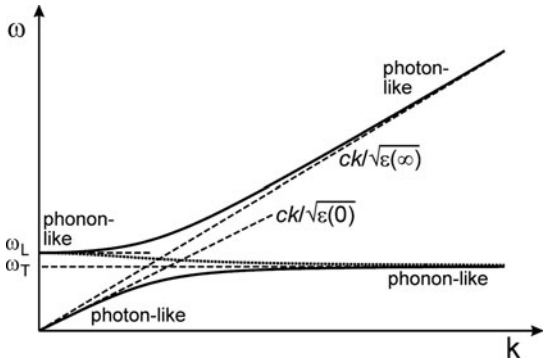

Fig. 9.41. Dispersion of the polariton. The *dotted line* displays the dispersion for a purely imaginary wavevector with the absolute value k

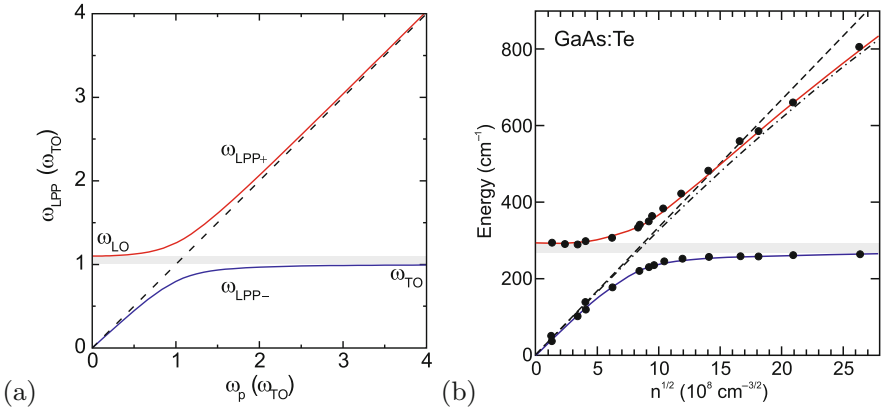

Fig. 9.42. (**a**) Frequency of the coupled longitudinal-phonon plasmon (LPP) modes (lower (upper) polariton branch in *blue* (*red*))as a function of the plasma frequency. *Dashed line* shows uncoupled plasmon frequency ($\omega = \omega_\mathrm{p}$), *grey area* indicates spectral region between TO and LO modes. (**b**) Experimental data on the polariton energies in n-type GaAs with different carrier concentration $\omega_\mathrm{p} \propto \sqrt{n\,m^*}$ (9.59). *Dashed* (*dash-dotted*) *line* is plasmon frequency ω_p without (with) consideration of conduction band non-parabolicity (cf. Fig. 6.26b). Data from [641, 645]

Both branches have a phonon- and a photon-like part. The coupled state between the phonon and the photon field is called the (phonon-) polariton.

In the interval $[\omega_\mathrm{TO}, \omega_\mathrm{LO}]$ the wavevector is purely imaginary, i.e. $k = \mathrm{i}\tilde{k}$ with real $\tilde{k}$. For this case there is only one solution that is also depicted in Fig. 9.41,

$$\omega^2 = \frac{1}{2}\left(\omega_\mathrm{LO}^2 + \frac{c^2\tilde{k}^2}{\epsilon(\infty)}\right) + \sqrt{\frac{1}{4}\left(\omega_\mathrm{LO}^2 + \frac{c^2\tilde{k}^2}{\epsilon(\infty)}\right)^2 + \left(\frac{c^2\tilde{k}^2\omega_\mathrm{TO}^2}{\epsilon(\infty)}\right)^2}\,. \quad (9.67)$$

9.8.4 Phonon–Plasmon Coupling

The coupling of phonons and plasmons in the spectral region of the reststrahlenbande leads to the development of two new branches, the longitudinal phonon plasmon modes (LPP+ and LPP−), in the common dispersion. The dielectric function is

$$\epsilon(\omega) = \epsilon(\infty)\left(1 + \frac{\omega_{\mathrm{LO}}^2 - \omega^2}{\omega_{\mathrm{TO}}^2 - \omega^2} - \frac{\omega_{\mathrm{p}}^2}{\omega^2}\right) . \tag{9.68}$$

For $\epsilon(\omega) = 0$ for $k = 0$ (coupling to photons) the two solutions $\omega_{\mathrm{LPP}+}$ and $\omega_{\mathrm{LPP}-}$ do not cross as a function of ω_{p} (Fig. 9.42),

$$\omega_{\mathrm{LPP}\pm} = \frac{1}{2}\left[\omega_{\mathrm{LO}}^2 + \omega_{\mathrm{p}}^2 \pm \sqrt{(\omega_{\mathrm{LO}}^2 + \omega_{\mathrm{p}}^2)^2 - 4\omega_{\mathrm{TO}}^2\omega_{\mathrm{p}}^2}\right] . \tag{9.69}$$

For small plasma frequencies $\omega_{\mathrm{LPP}+} = \omega_{\mathrm{LO}}$, i.e. the optical phonons couple to the electromagnetic field without change. Also $\omega_{\mathrm{LPP}-} = \omega_{\mathrm{p}}$. For large carrier density, i.e. $\omega_{\mathrm{p}} \gg \omega_{\mathrm{LO}}$, we find $\omega_{\mathrm{LPP}-} = \omega_{\mathrm{TO}}$ and $\omega_{\mathrm{LPP}+} = \omega_{\mathrm{p}}$. Thus, the carriers have effectively screened the electric field of the phonon that had led to the increase of the TO to the LO frequency.